

*Research Articles: Behavioral/Cognitive*

## Categorical Biases in Human Occipitoparietal Cortex

<https://doi.org/10.1523/JNEUROSCI.2700-19.2019>

**Cite as:** J. Neurosci 2019; 10.1523/JNEUROSCI.2700-19.2019

Received: 14 November 2019

Accepted: 3 December 2019

---

*This Early Release article has been peer-reviewed and accepted, but has not been through the composition and copyediting processes. The final version may differ slightly in style or formatting and will contain links to any extended data.*

**Alerts:** Sign up at [www.jneurosci.org/alerts](http://www.jneurosci.org/alerts) to receive customized email alerts when the fully formatted version of this article is published.

1 **Categorical Biases in Human Occipitoparietal Cortex**

2  
3 Edward F. Ester<sup>1\*</sup>, Thomas C. Sprague<sup>2</sup>, John T. Serences<sup>3</sup>

4  
5 <sup>1</sup>*Department of Psychology, Center for Complex Systems and Brain Sciences, and FAU Brain*  
6 *Institute, Florida Atlantic University*

7 <sup>2</sup>*Department of Psychological and Brain Sciences, University of California, Santa Barbara*

8 <sup>3</sup>*Department of Psychology, Neurosciences Graduate Program, and Kavli Institute for Brain and*  
9 *Mind, University of California, San Diego*

10  
11 \*Correspondence:

12  
13 Edward Ester

14 Department of Psychology, Center for Complex Systems and Brain Sciences, and FAU Brain Institute

15 Florida Atlantic University

16 777 Glades Rd.

17 Boca Raton, FL. 33431

18 eester@fau.edu

19  
20 **Acknowledgments:** Funding provided by NIH R01 EY025872 and a James S. McDonnell  
21 Foundation award to J.T.S.. E.F.E., conceived and designed the experiment, collected and  
22 analyzed the data, and wrote the paper. T.C.S. provided conceptual input during all phases of the  
23 project and edited the paper. J.T.S. supervised all phases of the project. The authors thank Kelvin  
24 Lam for assistance with data collection for Experiment 2. The authors declare no competing  
25 interests.

26  
27 **Word Counts:**

28  
29 Abstract: 183/250

30 Significance Statement: 93/120

31 Introduction: 463/650

32 Discussion: 1190/1500

33  
34 Figure/Table Count: 18/0

35

**Abstract**

36

37

38

39

40

41

42

43

44

45

46

47

48

49

50

51

52

53

Categorization allows organisms to generalize existing knowledge to novel stimuli and to discriminate between physically similar yet conceptually different stimuli. Humans, nonhuman primates, and rodents can readily learn arbitrary categories defined by low-level visual features, and learning distorts perceptual sensitivity for category-defining features such that differences between physically similar yet categorically distinct exemplars are enhanced while differences between equally similar but categorically identical stimuli are reduced. We report a possible basis for these distortions in human occipitoparietal cortex. In three experiments, we used an inverted encoding model to recover population-level representations of stimuli from multivoxel and multi-electrode patterns of human brain activity while human participants (both sexes) classified continuous stimulus sets into discrete groups. In each experiment, reconstructed representations of to-be-categorized stimuli were systematically biased towards the center of the appropriate category. These biases were largest for exemplars near a category boundary, predicted participants' overt category judgments, emerged shortly after stimulus onset, and could not be explained by mechanisms of response selection or motor preparation. Collectively, our findings suggest that category learning can influence processing at the earliest stages of cortical visual processing.

**Significance Statement**54  
55  
56  
57  
58  
59  
60  
61  
62  
63  
64

Category learning enhances perceptual sensitivity for physically similar yet categorically different stimuli. We report a possible mechanism for these changes in human occipitoparietal cortex. In three experiments, we used an inverted encoding model to recover population-level representations of stimuli from multivariate patterns in occipitoparietal cortex while participants categorized sets of continuous stimuli into discrete groups. The recovered representations were systematically biased by category membership, with larger biases for exemplars adjacent to a category boundary. These results suggest that mechanisms of categorization shape information processing at the earliest stages of the visual system.

65           Categorization refers to the process of mapping continuous sensory inputs onto discrete  
66 and behaviorally relevant concepts. It is a cornerstone of flexible behavior that allows organisms  
67 to generalize existing knowledge to novel stimuli and to discriminate between physically similar  
68 yet conceptually different stimuli. Many real-world categories are defined by a combination of  
69 low-level visual properties such as hue, luminance, spatial frequency, and orientation. For  
70 example, a forager might be tasked with determining whether a food source is edible based on  
71 subtle variations in color, shape, size, and texture. Humans and other animals can readily learn  
72 arbitrary novel categories defined by low-level visual properties (Goldstone, 1998; Ashby &  
73 Maddox, 2005), and such learning “distorts” perceptual sensitivity for category-defining features  
74 such that discrimination performance for physically similar yet categorically different stimuli is  
75 increased (i.e., acquired distinctiveness; Goldstone, 1995; Newell & Bulthoff, 2002) and  
76 discrimination performance for stimuli from the same category reduced (i.e., acquired similarity;  
77 Livingston et al., 1998).

78           Invasive electrophysiological studies suggest that single-unit responses in early visual  
79 areas index the physical properties of a stimulus but not its category membership, while single-  
80 unit responses in later areas index the category membership of a stimulus regardless of its  
81 physical properties (e.g., Sigala & Logothetis, 2002; Freedman et al., 2001; Freedman & Assad,  
82 2006). These results have been taken as evidence that category-selective responses are a *de novo*  
83 property of higher-order visual areas. However, perceptual distortions following category  
84 learning could also reflect subtle changes in how to-be-categorized information is represented by  
85 sensory neural populations (Folstein et al., 2012; Davis & Poldrack, 2013). Here we provide a  
86 test of this possibility. In three experiments, we trained human participants (both sexes) to  
87 classify sets of continuous stimuli into discrete groups. Next, next, we applied multivariate

88 models to noninvasive measurements of human brain activity (fMRI and EEG) from visual and  
89 parietal cortical areas while participants categorized the same stimulus sets. This allowed us to  
90 recover, visualize, and quantify stimulus-specific representations of to-be-categorized exemplars.  
91 In Experiment 1 (fMRI), we show that reconstructed representations of to-be-categorized  
92 orientations in visual areas V1-V3 are systematically biased towards the center of the category to  
93 which they belong. These biases were correlated with trial-by-trial variability in overt category  
94 judgments and were largest for orientations adjacent to the category boundary where they would  
95 be most beneficial for discrimination performance. In Experiment 2, we utilized EEG to generate  
96 time-resolved representations of to-be-categorized orientations and show that categorical biases  
97 manifest shortly after stimulus onset ( $\leq 300$  ms). In Experiment 3, we used EEG and a delayed  
98 match-to-category task to show that categorical biases observed in Experiments 1 and 2 cannot  
99 be explained by response biases or motor preparation. Collectively, our findings suggest that  
100 mechanisms of categorization can shape information processing at the earliest stages of the  
101 visual system.

102

103

**Methods**104 ***General Overview***

105 *Participants.* A total of 44 human volunteers (both sexes) participated in this study. Eight  
106 participants completed Experiment 1 (fMRI), 28 participants completed Experiment 2 (EEG),  
107 and eight participants completed Experiment 3 (EEG). Experiments 1 and 2 were performed at  
108 the University of California, San Diego, while Experiment 3 was performed at Florida Atlantic  
109 University. Participants were recruited from the student body at each university. All study  
110 procedures were approved by local institutional review boards, and all participants gave both  
111 written and oral informed consent. Participants self-reported normal or corrected-to-normal  
112 visual acuity and were remunerated with cash incentives (\$20/h for fMRI and \$15/h for EEG).

113 *Stimulus Displays.* Stimulus displays were generated in MATLAB and rendered using  
114 Psychophysics Toolbox software extensions (Kleiner et al., 2017). During Experiment 1 (fMRI),  
115 displays were projected onto a 110 cm-wide screen placed at the base of the MRI table, and  
116 participants viewed displays via a mirror attached to the MR head coil from a distance of 370  
117 cm. During Experiments 2 and 3, displays were projected onto a 19-inch CRT monitor cycling at  
118 120Hz (Experiment 2) or 85Hz (Experiment 3). Participants were seated approximately 65 cm  
119 from the display (head position was not constrained).

120 ***Experiment 1 - fMRI***

121 *Participants.* Eight neurologically intact human volunteers (AA, AB, AC, AD, AE, AF, AG, and  
122 AH; six females) completed Experiment 1. Each participant completed a single one-hour  
123 behavioral training session approximately 24-72 hours prior to scanning. Seven participants (AA,  
124 AB, AC, AD, AE, AF, AG) completed two 2-hour experimental scan sessions; an eighth  
125 participant (AH) completed a single 2-hour experimental scan session. Participants AA, AB, AC,

126 AD, AE, AF, and AH also completed a single 2-hour retinotopic mapping scan session. Data  
127 from this session were used to identify visual field borders in early visual cortical areas V1-  
128 hV4/V3A and subregions of posterior intraparietal sulcus (IPS0-3; see *Retinotopic Mapping*,  
129 below).

130 *Behavioral Tasks*. In separate runs (where “run” refers to a continuous block of 30 trials lasting  
131 280 seconds) participants performed either an orientation mapping task or a category  
132 discrimination task. Trials in each task lasted 3 seconds, and consecutive trials were separated by  
133 a 5 or 7 s inter-trial-interval (pseudorandomly chosen on each trial). During the orientation  
134 mapping task, participants attended a stream of letters presented at fixation (subtending  $1.0^\circ \times$   
135  $1.0^\circ$  from a viewing distance of 370 cm) while ignoring a task-irrelevant phase-reversing (15 Hz)  
136 square-wave grating (0.8 cycles/deg with inner and outer radii of  $1.16^\circ$  and  $4.58^\circ$ , respectively)  
137 presented in the periphery. On each trial, the grating was assigned one of 15 possible orientations  
138 ( $0^\circ$ - $168^\circ$  in  $12^\circ$  increments). Participants were instructed to detect and report the identity of a  
139 target (“X” or “Y”) in the letter stream using an MR-compatible button box. Only one target was  
140 presented on each trial. Letters were presented at a rate of 10 Hz (50% duty cycle, i.e. 50 msec  
141 on, 50 msec off), and targets could occur during any cycle from +750 to +2250 msec after  
142 stimulus onset. During category discrimination runs, participants were shown displays containing  
143 a circular aperture (inner and outer radii of  $1.16^\circ$  and  $4.58^\circ$  from a viewing distance of 370 cm)  
144 filled with 150 iso-oriented bars (see Figure 1A). Each bar subtended  $0.2^\circ \times 0.6^\circ$  with a stroke  
145 width of 8 pixels (1024 x 768 display resolution). Each bar flickered at 30 Hz and was randomly  
146 replotted within the aperture at the beginning of each “up” cycle.

147 On each trial, all bars were assigned an orientation from  $0^\circ$ - $168^\circ$  in  $12^\circ$  increments.

148 Inspired by earlier work in non-human primates (Freedman & Assad, 2006), we randomly



149 selected and designated one of these orientations as a category boundary such that the seven  
150 orientations counterclockwise to this value were assigned membership in “Category 1”, while the  
151 seven orientations clockwise to this value were assigned membership in “Category 2”.

152 Participants were not informed that the category boundary was chosen from the set of possible  
153 stimulus orientations. Participants reported whether the orientation shown on each trial was a  
154 member of Category 1 or 2 (via an MR-compatible button box). Participants were free to respond  
155 at any point during the trial, though the stimulus was always presented for a total of 3000 ms.

156 Each participant was familiarized and trained to criterion performance on the category  
157 discrimination task during a one-hour behavioral testing session completed one to three days  
158 prior to his or her first scan session. Written feedback (“Correct!” or “Incorrect”) was presented  
159 in the center of the display for 1.25 sec. after each trial during behavioral training and MR  
160 scanning. Across either one (N = 1) or two (N = 7) scan sessions, each participant completed 7  
161 (N = 1), 13 (N = 1), 14 (N = 1), 15 (N = 1) or 16 (N = 4) runs of the orientation mapping and  
162 category discrimination tasks.

163 *fMRI Acquisition and Preprocessing.* Imaging data were acquired with a 3.0T GE MR 750  
164 scanner located at the Center for Functional Magnetic Resonance imaging on the UCSD campus.  
165 All images were acquired with a 32 channel Nova Medical head coil (Wilmington, MA). Whole-  
166 brain echo-planar images (EPIs) were acquired in 35 3 mm slices (no gap) with an in-plane  
167 resolution of 3 x 3 mm (192 x 192 mm field-of-view, 64 x 64 mm image matrix, 90° flip angle,  
168 2000 ms TR, 30 ms TE). During retinotopic mapping scans (see below) EPIs were acquired in 31  
169 3mm thick oblique slices (no gap) positioned over posterior visual and parietal cortex with an in-  
170 plane resolution of 2 x 2 mm (192 x 192 mm field-of-view, 96 x 96 mm image matrix, 90° flip  
171 angle, 2250 ms TR, 30 ms TE). EPIs were coregistered to a high-resolution anatomical image

172 collected during the same session (FSPGR T1-weighted sequence, 11 ms TR, 3.3 ms TE, 1100  
173 ms TI, 172 slices, 18° flip angle, 1 mm<sup>3</sup> resolution), unwarped (FSL software extensions), slice-  
174 time-corrected, motion-corrected, high-pass-filtered (to remove first-, second- and third-order  
175 drift), transformed to Talairach space, and normalized (z-score) on a scan-by-scan basis. Data  
176 from data from scan sessions were then co-registered to a high-resolution anatomical image  
177 (FSPGR T1-weighted sequences; parameters as described above) collected during the retinotopic  
178 mapping session.

179 *Retinotopic Mapping.* Retinotopically organized visual areas V1-hV4v/V3A were defined using  
180 data from a single retinotopic mapping run collected during each experimental scan session.

181 Participants fixated a small dot at fixation while phase-reversing (8 Hz) checkerboard wedges  
182 subtending 60° of polar angle (at maximum eccentricity) were presented along the horizontal or  
183 vertical meridian (alternating with a period of 40 seconds; i.e., 20 seconds of horizontal  
184 stimulation followed by 20 seconds of vertical stimulation). To identify visual field borders, we  
185 constructed a general linear model with two boxcar regressors, one marking epochs of vertical  
186 stimulation and another marking epochs of horizontal stimulation. Each regressor was convolved  
187 with a canonical hemodynamic function (“double gamma” as implemented in BrainVoyager  
188 QX). Next, we generated a statistical parametric map marking voxels with larger responses  
189 during epochs of vertical relative to horizontal stimulation. This map was projected onto a  
190 computationally inflated representation of each participant’s cortical surface for visualization to  
191 aid in the definition of the borders of visual areas V1, V2v, V2d, V3v, V3d, hV4v, and V3A.

192 Data from V2v and V2d were combined into a single V2 ROI, and data from V3v and V3d were  
193 combined into a single V3 ROI. ROIs were also combined across cortical hemispheres (e.g., left

194 and right V1) as no asymmetries were observed and the stimulus was presented in the center of  
195 the visual field.

196         Seven participants (AA, AB, AC, AD, AE, AF, and AH) completed a separate two-hour  
197 retinotopic mapping scan; data from this session were used to identify retinotopically organized  
198 regions of inferior parietal sulcus (IPS0-3). During each task run, participants were shown  
199 displays containing a rotating wedge stimulus (period 24.75 or 36 sec) that subtended 72° of  
200 polar angle with inner and outer radii of 1.75 and 8.75°, respectively. In alternating blocks, the  
201 wedge contained a 4 Hz phase-reversing checkerboard or field of moving dots and participants  
202 were required to detect small, brief, and temporally unpredictable changes in checkerboard  
203 contrast or dot speed. Six participants completed between 8 and 14 task runs. To compute the  
204 best polar angle for each voxel in IPS we shifted the signals from counterclockwise runs by twice  
205 the estimated hemodynamic response function (HRF) delay ( $2 \times 6.75 \text{ s} = 13.5 \text{ s}$ ), removed data  
206 from the first and last full stimulus cycle, and reversed the time series so that all runs reflected  
207 clockwise rotation. We next computed the power and phase of the response at the stimulus'  
208 period (either 1/24.75 or 1/36 Hz) and subtracted the estimated hemodynamic response function  
209 delay (6.75 seconds) to align the signal phase in each voxel with the stimulus' location. Maps of  
210 orientation preference (computed via cross-correlation) were projected onto a computationally  
211 inflated representation of each participant's grey-white matter boundary to aide in the  
212 identification of visual field borders separating IPS0-3. An eighth participant (AG) chose not to  
213 participate in an additional retinotopic mapping session. For this participant, we estimated visual  
214 field borders for visual areas V1-hV4/V3A. using data from the retinotopic mapping run  
215 collected during the participant's sole experimental session. We did not attempt to define IPS  
216 regions IPS0-3 for this participant.

217 *Decoding Categorical Biases in Visual Cortex.* We used a linear decoder to examine whether  
218 fMRI activation patterns evoked by exemplars adjacent to the category boundary and at the  
219 center of each category were more similar during the category discrimination task relative to the  
220 orientation mapping task (i.e., acquired similarity). In the first phase of the analysis, we trained a  
221 linear support vector machine (LIBSVM implementation; Chang & Lin, 2011) to discriminate  
222 between the oriented exemplars at the center of each category ( $48^\circ$  from the boundary) using  
223 data from the orientation mapping and category discrimination tasks. To ensure internal  
224 reliability, we implemented a “leave-one-run-out” cross validation scheme where data from all  
225 but one scanning run was used to train the classifier and data from the remaining scanning run  
226 were used for validation. This procedure was repeated until data from each scan had served as  
227 the validation set, and the results were averaged across permutations. Next, we trained a second  
228 classifier on activation patterns evoked by exemplars at the center of each category boundary and  
229 used the trained classifier to predict the category membership of exemplars adjacent to the  
230 category boundary. If category learning increases the similarity of activation patterns evoked by  
231 exemplars within the same category, then within-category decoding performance should be  
232 superior during the category discrimination task relative to the orientation mapping task.

233 *Inverted Encoding Model of Orientation Selectivity.* A linear inverted encoding model (IEM)  
234 was used to recover a model-based representation of stimulus orientation from multivoxel  
235 activation patterns measured in early visual areas (Brouwer & Heeger, 2011). The same general  
236 approach was used during Experiments 1 (fMRI) and 2 (EEG). Specifically, we modeled the  
237 responses of voxels (electrodes) measured during the orientation mapping task as a weighted  
238 sum of 15 orientation-selective channels, each with an idealized response function (half-wave-  
239 rectified sinusoid raised to the 14<sup>th</sup> power). The maximum response of each channel was set to

240 unit amplitude; thus units of response are arbitrary. Let  $B_1$  ( $m$  voxels or electrodes  $\times$   $n_1$  trials) be  
 241 the response of each voxel (electrode) during each trial of the RSVP task, let  $C_1$  ( $k$  filters  $\times$   $n_1$   
 242 trials) be a matrix of hypothetical orientation filters, and let  $W$  ( $m$  voxels or electrodes  $\times$   $k$  filters)  
 243 be a weight matrix describing the mapping between  $B_1$  and  $C_1$ :

244

$$B_1 = WC_1$$

245

246 In the first phase of the analysis, we computed the weight matrix  $W$  from the voxel-wise  
 247 (electrode-wise) responses in  $B_1$  via ordinary least-squares:

248

$$W = B_1 C_1^T (C_1 C_1^T)^{-1}$$

249

250 Next, we defined a test data set  $B_2$  ( $m$  voxels or electrodes  $\times$   $n_2$  trials) using data from the  
 251 category discrimination task. Given  $W$  and  $B_2$ , a matrix of filter responses  $C_2$  ( $k$  filters  $\times$   $n$  trials)  
 252 can be estimated via model inversion:

253

$$C_2 = (W^T W)^{-1} W^T B_2$$

254

255  $C_2$  contains the reconstructed response of each modeled orientation channel (the channel  
 256 response function; CRF) on each trial of the category discrimination task. This analysis can be  
 257 considered a form of model-based, directed dimensionality reduction where activity patterns are  
 258 transformed from their original measurement space (fMRI voxels; EEG electrodes) into a  
 259 modeled information space (orientation-selective channels). Importantly, results from this

260 method cannot be used to infer any changes in orientation tuning – or any properties of neural  
261 responses - occurring at the single neuron level, and only assay the information content of large-  
262 scale patterns of neural activity (Sprague et al., 2018) Additionally, while it is the case that  
263 arbitrary linear transforms can be applied to the basis set, model weights, and reconstructed  
264 channel response function (Gardiner & Liu, 2019), results are uniquely defined for a given model  
265 specification (Sprague, Boynton & Serences, 2019). Trial-by-trial CRFs were multiplied by the  
266 original basis set to recover a full 180-degree function, circularly shifted to a common center ( $0^\circ$ )  
267 and sorted by category membership so that any category bias would manifest as a clockwise shift  
268 (i.e., towards the center of Category 2).

269 *Quantification of Bias in Orientation Representations.* To quantify categorical biases in  
270 reconstructed model-based CRFs, these functions were fit with an exponentiated cosine function  
271 of the form:

272

$$f(x) = \alpha(e^{k(\cos(\mu-x)-1)}) + \beta$$

273

274 where,  $x$  is a vector of channel responses and  $\alpha$ ,  $\beta$ ,  $k$  and  $\mu$  correspond to the amplitude (i.e.,  
275 signal over baseline), baseline, concentration (the inverse of bandwidth) and the center of the  
276 function, respectively. Fitting was performed using a multidimensional nonlinear minimization  
277 algorithm (Nelder-Mead).

278 Category biases in the estimated center of each construction ( $\mu$ ) during the category  
279 discrimination task were quantified via permutation tests. For a given visual area (e.g., V1) we  
280 randomly selected (with replacement) stimulus reconstructions from eight of eight participants.  
281 Specifically, we computed a “mean” reconstruction by randomly selecting (with replacement)

282 and averaging reconstructions from all participants. The mean reconstruction was fit with the  
283 cosine function described above, yielding point estimates of  $\alpha$ ,  $\beta$ ,  $k$ , and  $\mu$ . This procedure was  
284 repeated 1,000 times, yielding 1,000 element distributions of parameter estimates. We then  
285 computed the proportion of permutations where a  $\mu$  value less than 0 was obtained to obtain an  
286 empirical  $p$ -value for categorical shifts in reconstructed representations.

287 *Searchlight Decoding of Category Membership.* We used a roving searchlight analysis (Ester et  
288 al., 2015) to identify cortical regions beyond V1-V3 that contained category-specific  
289 information. We defined a spherical neighborhood with a radius of 8 mm around each grey  
290 matter voxel in the cortical sheet. We next extracted and averaged the normalized response of  
291 each voxel in each neighborhood over a period from 4-8 seconds after stimulus onset (this  
292 interval was chosen to account for typical hemodynamic lag of 4-6 seconds). A linear SVM  
293 (LIBSVM implementation) was used to classify stimulus category using activation patterns  
294 within each neighborhood. To classify category membership, we designated the three  
295 orientations immediately counterclockwise to the category boundary (see Figure 1) as members  
296 of Category 1 and the three orientations immediately clockwise of the boundary as members of  
297 Category 2. We then trained our classifier to discriminate between categories using data from all  
298 but one task run. The trained classifier was then used to predict category membership from  
299 activation patterns measured during the held-out task run. This procedure was repeated until each  
300 task run had been held out, and the results were averaged across permutations. Finally, we  
301 repeated the same analysis using the three Category 1 and Category 2 orientations adjacent to the  
302 second (orthogonal) category boundary (see Figure 1) and averaged the results across category  
303 boundaries.

304 We identified neighborhoods encoding stimulus category using a leave-one-participant-  
305 out cross validation approach (Esterman et al., 2010). Specifically, for each participant (e.g., AA)  
306 we randomly selected (with replacement) and averaged classifier performance estimates from  
307 each neighborhood from each of the remaining 7 volunteers (e.g., AB-AH). This procedure was  
308 repeated 1000 times, yielding a set of 1000 classifier performance estimates for each  
309 neighborhood. We generated a statistical parametric map (SPM) for the held-out participant that  
310 indexed neighborhoods where classifier performance was greater than chance (50%) on 97.5% of  
311 permutations (false-discovery-rate corrected for multiple comparisons across neighborhoods).  
312 Finally, we projected each participant's SPM onto a computationally inflated representation of  
313 his or her grey-white matter boundary and used Brain Voyager's "Create POIs from Map  
314 Clusters" function with an area threshold of 25 mm<sup>2</sup> to identify ROIs supporting above-chance  
315 category classification performance. Because of differences in cortical folding patterns, some  
316 ROIs could not be unambiguously identified in all 8 participants. Therefore, across participants,  
317 we retained all ROIs that were shared by at least 7 out of 8 participants. Finally, we extracted  
318 multivoxel activation patterns from each ROI and computed model-based reconstructions of  
319 channel response functions during the RSVP and category tasks using a leave-one-run-out cross-  
320 validation approach. Specifically, we used data from all but one task run to estimate a set of  
321 orientation weights for each voxel in each ROI. We then used these weights and activation  
322 patterns measured during the held-out task run to estimate a channel response function, which  
323 contains a representation of stimulus orientation. This procedure was repeated until each task run  
324 had been held out, and the results were averaged across permutations. Note that each  
325 participant's ROIs were defined using data from the remaining 7 participants. This ensured that



326 participant-level reconstructions were statistically independent of the searchlight method used to  
327 define ROIs encoding category information.

328 *Within-participant Error Bars.* We report estimates of within-participant variability (e.g.,  $\pm 1$   
329 S.E.M.) throughout the paper. These estimates discard subject variance (e.g., overall differences  
330 in BOLD response amplitude) and instead reflect variance related to the subject by condition(s)  
331 interaction term(s) (i.e., variability in estimated channel responses). We used the approach  
332 described by Cousineau (2005): raw data (e.g., channel response estimates) were de-meaned on a  
333 participant by participant basis, and the grand mean across participants was added to each  
334 participant's zero-centered data. The grand mean-centered data were then used to compute  
335 estimates of standard error.

### 336 **Experiment 2 - EEG**

337 *Participants.* 29 new volunteers recruited from the UC San Diego community completed  
338 Experiment 2. All participants self-reported normal or corrected-to-normal visual acuity and  
339 gave both written and oral informed consent as required by the local Institutional Review Board.  
340 Each participant was tested in a single 2.5-3 hour experimental session (the exact duration varied  
341 across participants depending on the amount of time needed to set up and calibrate the EEG  
342 equipment). Unlike Experiment 1, participants were not trained on the categorization task prior  
343 to testing. We adopted this approach in the hopes of tracking the gradual emergence of  
344 categorical biases during learning. However, many participants learned the task relatively  
345 quickly (within 40-60 trials), leaving too few trials to enable a direct analysis of this possibility.  
346 Data from one participant were discarded due to a high number of EOG artifacts (over 35% of  
347 trials); the data reported here reflect the remaining 28 participants.

348 *Behavioral Tasks.*

349 In separate runs (where “run” refers to a continuous block of 60 trials lasting approximately 6.5  
350 minutes), participants performed orientation mapping and category discrimination tasks similar  
351 to those used in Experiment 1. During both tasks a rapid series of letters (subtending  $1.14^\circ \times$   
352  $1.14^\circ$  from a viewing distance of 55 cm) was presented at fixation, and an aperture of 150 iso-  
353 oriented bars (subtending  $0.5^\circ \times 1.2^\circ$ ) was presented in the periphery. The aperture of bars had  
354 inner and outer radii of  $1.96^\circ$  and  $9.13^\circ$ , respectively. On each trial, the bars were assigned one of  
355 15 possible orientations (again  $0^\circ$ - $168^\circ$  in  $12^\circ$  increments) and flickered at a rate of 30 Hz. Each  
356 bar was randomly replotted within the aperture at the beginning of each “up” cycle. Letters in the  
357 RSVP stream were presented at a rate of 6.67 Hz

358       During orientation mapping runs, participants detected and reported the presence of a  
359 target letter (an X or Y) that appeared at an unpredictable time during the interval from +750  
360 msec to +2250 ms following stimulus onset. Responses were made on a USB-compatible  
361 number pad. During category discrimination runs, participants ignored the RSVP stream and  
362 instead reported whether the orientation of the bar aperture was an exemplar from category “1”  
363 or category “2”. As in Experiment 1, we randomly designated one of the 15 possible stimulus  
364 orientations as the category boundary such that the seven orientations counterclockwise to this  
365 value were assigned to Category 1 and the seven orientations clockwise to this value were  
366 assigned to Category 2. Participants could respond at any point during the trial, but the stimulus  
367 was presented for a total of 3000 msec. Trials were separated by a 2.5 – 3.25 sec inter-trial-  
368 interval (randomly selected from a uniform distribution on each trial). Each participant  
369 completed four (N = 1), five (N = 10), six (N = 8), seven (N = 8), or eight (N = 1) blocks of the  
370 category task and three (N = 1), four (N = 1), five (N = 5), six (N = 12), seven (N = 8), or eight  
371 (N = 1) blocks of the orientation mapping task.

372 *EEG Acquisition and Preprocessing.* Participants were seated in a dimly lit, sound-attenuated,  
373 and electrically shielded recording chamber (ETS Lindgren) for the duration of the experiment.  
374 Continuous EEG was recorded from 128 Ag-AgCl<sup>+</sup> scalp electrodes via a Biosemi “Active Two”  
375 system (Amsterdam, Netherlands). The horizontal electrooculogram (EOG) was recorded from  
376 additional electrodes placed near the left and right canthi, and the vertical EOG was recorded  
377 from electrodes placed above and below the right eye. Additional electrodes were placed over  
378 the left and right mastoids. The horizontal and vertical EOG were recorded from electrodes  
379 placed over the left and right canthi and above and below the right eye (respectively). Electrode  
380 impedances were kept well below 20 k $\Omega$ , and recordings were digitized at 1024 Hz.

381       After testing, the entire EEG time series at each electrode was high- and low-pass filtered  
382 (3<sup>rd</sup> order zero-phase forward and reverse Butterworth) at 0.1 and 50 Hz and re-referenced to the  
383 average of the left and right mastoids. Data from both tasks were epoched into intervals spanning  
384 -1000 to +4000 msec from stimulus onset; the relatively large pre- and post-stimulus epochs  
385 were included to absorb filtering artifacts that could affect later analyses. Trials contaminated by  
386 EOG artifacts (horizontal eye movements > 2° and blinks) were identified and excluded from  
387 additional analyses. Across participants an average of 5.58% ( $\pm$ 1.67%) and 8.74% ( $\pm$ 1.84%) of  
388 trials from the orientation mapping and category discrimination tasks were discarded  
389 (respectively). Finally, noisy channels (those with multiple deflections  $\geq$  100  $\mu$ V over the course  
390 of the experiment) were visually identified and eliminated (mean number of removed electrodes  
391 across participants  $\pm$ 1 S.E.M. = 2.25  $\pm$  0.64).

392       Next, we identified a set of electrodes-of-interest (EOIs) with strong responses at the  
393 stimulus’ flicker frequency (30 Hz). Data from each task were re-epoched into intervals spanning  
394 0 to 3000 msec around stimulus onset and averaged across trials and tasks (i.e., RSVP and

395 category discrimination), yielding a  $k$  electrode by  $t$  sample data matrix. We computed the  
396 evoked power at the stimulus' flicker frequency (30 Hz) by applying a discrete Fourier transform  
397 to the average time series at each electrode and selected the 32 electrodes with the highest  
398 evoked power at the stimulus' flicker frequency for further analysis. These electrodes were  
399 typically distributed over occipitoparietal electrode sites (see Figure 12).

400 To isolate stimulus-specific responses, the epoched timeseries at each electrode was  
401 resampled to 256 Hz and then bandpass filtered from 29 to 31 Hz (zero-phase forward and  
402 reverse 3<sup>rd</sup> order Butterworth). We next estimated a set of complex Fourier coefficients  
403 describing the power and phase of the 30 Hz response by applying a Hilbert transformation to the  
404 filtered data. To visualize and quantify orientation-selective signals from frequency-specific  
405 responses, we first constructed a complex-valued data set  $B_1(t)$  ( $m$  electrodes  $\times$   $n_{train}$  trials). We  
406 then estimated a complex-valued weight matrix  $W(t)$  ( $m$  channels  $\times$   $k$  filters) using  $B_1(t)$  and a  
407 basis set of idealized orientation-selective filters  $C_1$ . Finally, we estimated a complex-valued  
408 matrix of channel responses  $C_2(t)$  ( $m$  channels  $\times$   $n_{test}$  trials) given  $W(t)$  and complex-valued test  
409 data set  $B_2(t)$  ( $m$  electrodes  $\times$   $n_{test}$  trials) containing the complex Fourier coefficients measured  
410 during the category discrimination task. Trial-by-trial and sample-by-sample response functions  
411 were shifted in the same manner described above so that category biases would manifest as a  
412 rightward (clockwise) shift towards the center of Category 2. We estimated the evoked (i.e.,  
413 phase-locked) power of the response at each filter by computing the squared absolute value of  
414 the average complex-valued coefficient for each filter after shifting. Categorical biases were  
415 quantified using the same curve fitting analysis described in the main text.

416 To obtain an unbiased estimate of orientation selectivity in each electrode, we ensured  
417 that the training data set  $B_1(t)$  contained an equal number of trials for each stimulus orientation

418 (0-168° in 12° increments). For each participant, we identified the stimulus orientation  $\theta$  with the  
419  $N$  fewest repetitions in the orientation mapping data set after EOG artifact removal. Next, we  
420 constructed the training data set  $B_1(t)$  by randomly selecting (without replacement)  $1:N$  trials for  
421 each stimulus orientation. Data from this training set were used to estimate a set of orientation  
422 weights for each electrode and these weights were in turn used to estimate a response for each  
423 hypothetical orientation channel during the category discrimination task. To ensure that our  
424 method generalized across multiple combinations of orientation mapping trials, we repeated this  
425 analysis 100 times and averaged the results across permutations.

### 426 **Experiment 3 - EEG**

427 *Participants.* 8 volunteers recruited from the Florida Atlantic University community completed  
428 Experiment 3. All participants self-reported normal or corrected-to-normal visual acuity and  
429 gave both written and oral informed consent as required by the local Institutional Review Board.  
430 Each participant was tested in a single 2-2.5 hour experimental session (the exact duration varied  
431 across participants depending on the amount of time needed to set up and calibrate the EEG  
432 equipment).

433 *Behavioral Tasks.* Participants performed six blocks of a spatial recall task followed by multiple  
434 blocks of a delayed match-to-category (DMC) task. Both tasks used identical stimulus and  
435 display geometry. During the spatial recall task, participants were shown a sample display  
436 containing a disc (diameter 2.5° from a viewing distance of 60 cm) rendered in one of 12 polar  
437 locations (0° to 330° in 30° increments) along the perimeter of an imaginary circle centered at  
438 fixation (radius 7.5°). The sample display was shown for 250 ms and followed by a 1750 ms  
439 blank delay. At the end of each trial, participants were shown a mouse cursor and instructed to  
440 click on the position of the disc shown in the sample display. Participants were instructed to

441 prioritize accuracy over speed, though a 3000 ms response deadline was imposed. Each trial was  
442 followed by a 1500-2200 ms blank interval (randomly sampled from a uniform distribution on  
443 each trial). Each block featured 72 trials (six repetitions per stimulus position) and lasted  
444 approximately six minutes. EEG data recorded during this task were used to train a position-  
445 specific inverted encoding model (see below). Each participant completed six blocks of this task.

446         After completing the spatial recall task, participants performed a delayed match-to-  
447 category task. Participants were shown stimuli in the same 12 positions used during the spatial  
448 recall task. However, for each participant we defined a category boundary such that half of the  
449 possible stimulus positions were assigned membership in Category 1 and the remaining half  
450 were assigned membership in Category 2. For example, the category boundary could be set such  
451 that positions [315, 345, 15, 45, 75, 105] comprised Category 1 while positions [135, 165, 195,  
452 225, 255, 285] comprised Category 2. The location of the category boundary was randomly and  
453 independently chosen for each participant and held constant throughout the experiment. At the  
454 beginning of each trial, a sample disc appeared in one of the 12 possible stimulus locations for  
455 250 ms. After a 1750 ms delay period, a probe disc was presented. The probe could occupy any  
456 of the 11 stimulus positions not occupied by the sample, and participants were required to judge  
457 whether the position of the probe matched the category of the sample stimulus via keypress.  
458 Participants were instructed to prioritize accuracy over speed, but a 3000 ms response limit was  
459 imposed. Feedback (correct vs. incorrect) was presented at the end of each trial. Participants  
460 completed 5 (N = 1) or 8 (N = 7) blocks of 72 trials.

461         *EEG Acquisition and Preprocessing.* Continuous EEG was recorded from 63 Ag/Ag-Cl  
462 scalp electrodes via a Brain Products actiCHamp amplifier. An additional electrode was placed  
463 over the right mastoid. Data were recorded with a right mastoid reference and later re-referenced

464 to the algebraic mean of the left and right mastoids (10-20 site TP9 served as the left mastoid  
465 reference). The horizontal and vertical electrooculogram (EOG) was recorded from electrodes  
466 placed on the left and right canthi and above and below the right eye, respectively. All electrode  
467 impedances were kept below 15 k $\Omega$ , and recordings were digitized at 1000 Hz. Recorded data  
468 were bandpass filtered from 1 to 50 Hz (3<sup>rd</sup> order zero-phase forward and reverse Butterworth  
469 filters), epoched from a period spanning -1000 to +3000 ms relative to the start of each trial, and  
470 baseline corrected from -250 to 0 ms. Muscle and electrooculogram artifacts were removed from  
471 the data using independent components analysis (ICA) as implemented in EEGLAB (Delorme &  
472 Makeig, 2004). Reconstructions of stimulus locations were computed from the spatial  
473 topography of induced alpha-band (8-12 Hz) power measured across 17 occipitoparietal  
474 electrode sites: O1, O2, Oz, PO7, PO3, POz, PO4, PO8, P7, P5, P3, P1, Pz, P2, P4, P6, and P8.  
475 *Inverted Encoding Model*. Experiment 3 relied on a fundamentally different signal than  
476 Experiment 2 (induced-alpha-band activity vs. evoked 30 Hz power, respectively). Following  
477 earlier research (Kok et al., 2017; Ester et al., 2018; Nouri & Ester, 2019), we used a variant of  
478 the IEM approach described in Experiment 2 to compute location channel responses. We first  
479 isolated alpha-band activity, by bandpass filtering the raw EEG time series at each electrode  
480 from 8-12 Hz (zero-phase forward and reverse filters as implemented by EEGLAB's "eegfilt"  
481 function), yielding a real-valued signal  $f(t)$ . The analytic representation of  $f(t)$  was obtained by  
482 applying a Hilbert transformation:

483

$$z(t) = f(t) + if(t)$$

484

485 where  $i = \sqrt{-1}$  and  $if(t) = A(t)e^{i\varphi(t)}$ . Induced alpha power was computed by extracting and  
486 squaring the instantaneous amplitude  $A(t)$  of the analytic signal  $z(t)$ . We modeled alpha power at  
487 each scalp electrode as a weighted sum of 12 location-selective channels, each with an idealized  
488 tuning curve (a half-wave rectified cosine raised to the 12<sup>th</sup> power). The maximum response of  
489 each channel was normalized to 1, thus units of response are arbitrary. The predicted responses  
490 of each channel during each trial were arranged in a  $k$  channel by  $n$  trials design matrix  $C$ .  
491 Separate design matrices were constructed to track the locations of the blue and red discs across  
492 trials (i.e., we reconstructed the locations of the blue and red discs separately, then later sorted  
493 these reconstructions according to cue condition). The relationship between the data and the  
494 predicted channel responses  $C$  is given by a general linear model of the form:

495

$$B = WC + N$$

496

497 where  $B$  is a  $m$  electrode by  $n$  trials training data matrix,  $W$  is an  $m$  electrode by  $k$  channel weight  
498 matrix, and  $N$  is a matrix of residuals (i.e., noise).

499 To estimate  $W$ , we constructed a “training” data set containing an equal number of trials  
500 from each stimulus location (i.e., 45-360° in 45° steps) condition. We first identified the location  
501  $\varphi$  with the fewest  $r$  repetitions in the full data set after EOG artifact removal. Next, we  
502 constructed a training data set  $B_{rm}$  ( $m$  electrodes by  $n$  trials) and weight matrix  $C_{rm}$  ( $n$  trials by  $k$   
503 channels) by randomly selecting (without replacement)  $1:r$  trials for each of the eight possible  
504 stimulus locations (ignoring cue condition; i.e., the training data set contained a mixture of  
505 neutral and valid trials). The training data set was used to compute a weight for each channel  $C_i$   
506 via least-squares estimation:



507

$$W_i = B_{trn} C_{trn,i}^T (C_{trn,i} C_{trn,i}^T)^{-1}$$

508

509 where  $C_{trn,i}$  is an  $n$  trial row vector containing the predicted responses of spatial channel  $i$  during  
 510 each training trial.

511 After estimating the weight matrix  $W$ , we next estimated a set of spatial filters  $V$  that  
 512 capture the underlying channel responses while accounting for correlated variability between  
 513 electrode sites (i.e., the noise covariance; Kok et al. 2017):

514

$$V_i = \frac{\Sigma_i^{-1} W_i}{W_i^T \Sigma_i^{-1} W_i}$$

515

516 where  $\Sigma_i$  is the regularized noise covariance matrix for channel  $i$  and estimated as:

517

$$\Sigma_i = \frac{1}{n-1} \epsilon_i \epsilon_i^T$$

518

519 where  $n$  is the number of training trials and  $\epsilon_i$  is a matrix of residuals:

520

$$\epsilon_i = B_{trn} - W_i C_{trn,i}$$

521

522 Estimates of  $\epsilon_i$  were obtained by regularization-based shrinkage using an analytically  
 523 determined shrinkage parameter (see Blankertz et al. 2011; Kok et al. 2017). An optimal spatial  
 524 filter  $v_i$  was estimated for each channel  $C_i$ , yielding an  $m$  electrode by  $k$  filter matrix  $V$ . Next, we

525 constructed a “test” data set  $B_{tst}$  ( $m$  electrodes by  $n$  trials) containing data from all trials not  
526 included in the training data set and estimated trial-by-trial channel responses  $C_{tst}$  ( $k$  channels x  $n$   
527 trials) from the filter matrix  $V$  and the test data set:

528

$$C_{tst} = V^T B_{tst}$$

529

530 Trial-by-trial channel responses were interpolated to  $360^\circ$ , circularly shifted to a common  
531 center ( $0^\circ$ , by convention), and sorted by category membership. As in Experiments 1 and 2,  
532 reconstructions were shifted and aligned so that any bias would manifest as a shift toward  
533 Category B (clockwise). Finally, to ensure internal reliability this entire analysis was repeated 50  
534 times, and unique (randomly chosen) subsets of trials were used to define the training and test  
535 data sets during each permutation. The results were then averaged across permutations.

536 *Eye Movement Control Analyses – Experiments 2 and 3.* Systematic biases in eye position can  
537 contribute to orientation and location performance (e.g., Quax et al., 2019). We did not collect  
538 eye position data from Experiment 1 (fMRI). However, different tasks were used to train and test  
539 the encoding model, which can be an effective way of mitigating the effects of eye movements  
540 on stimulus decoding (Mostert et al., 2018). We also collected electrooculogram (EOG) data  
541 during Experiments 2 and 3 (EEG). To examine whether eye position varied as a function of  
542 stimulus position during these experiments, we regressed trial-by-trial horizontal EOG  
543 recordings (in  $\mu\text{V}$ ) onto the orientation of a to-be-categorized stimulus (Experiment 2) or the  
544 location of a to-be-categorized disc (Experiment 3). In both experiments, we identified and  
545 excluded trials contaminated by large horizontal EOG artifacts ( $\geq 40 \mu\text{V}$ , which corresponds to a  
546 horizontal displacement of  $2.5^\circ$  assuming a voltage threshold of  $16 \mu\text{V}$  per degree; Lins et al.,

547 1993), but smaller variations in eye positions – for example, along the inner stimulus aperture –  
548 may have escaped detection. Using Experiment 2 as an example, we considered two possibilities.  
549 First, participants may have foveated the inner aperture of the stimulus at a polar location  
550 matching its orientation. To illustrate, participants could foveate the inner aperture of a 45°  
551 stimulus at a polar angle of 45° or 225°; likewise, they could foveate the inner aperture of a 168°  
552 stimulus at a polar angle of 168° or 348°. Second, participants may have foveated the inner  
553 aperture of each stimulus matching the center of the category it belonged to. We tested these  
554 possibilities by calculating predicted horizontal eye positions under the assumption that  
555 participants foveated the inner stimulus aperture at locations matching its orientation or the  
556 center of the relevant category. Specifically, we converted records of stimulus orientation (or the  
557 center of the category to which the stimulus belonged) to polar format and scaled the resulting  
558 estimates by the radius of the inner stimulus aperture, then regressed these estimates onto  
559 horizontal EOG activity (in  $\mu\text{V}$ ). If there is a systematic relationship between eye position and  
560 either stimulus orientation or category at any point during a trial, then this analysis should yield  
561 regression coefficients reliably greater than 0  $\mu\text{V}$ . Identical analyses were used to examine  
562 systematic relationships between horizontal eye position and stimulus location in Experiment 3.  
563  
564

565

**Results**566 *Experiment 1 - fMRI*

567 We trained eight human volunteers to categorize a set of orientations into two groups, Category 1  
568 and Category 2. The stimulus space comprised a set of 15 oriented stimuli, spanning 0-168° in  
569 12° increments (Figure 1A-B). For each participant, we randomly designated one of these 15  
570 orientations as a category boundary such that the seven orientations anticlockwise to the  
571 boundary were assigned membership in Category 1 and the seven orientations clockwise to the  
572 boundary were assigned membership in Category 2. Each participant completed a one-hour  
573 training session prior to scanning. Each participant's category boundary was kept constant across  
574 all behavioral training and scanning sessions. Many participants self-reported that they learned  
575 the rule delineating the categories in one or two 5-minute blocks of trials. Consequently, task  
576 performance measured during scanning was extremely high, with errors and slow responses  
577 present only for exemplars immediately adjacent to the category boundary (Figure 1C-D).  
578 During each scanning session, participants performed the category discrimination task and an  
579 orientation model estimation task where they were required to report the identity of a target letter  
580 embedded within a rapid stream presented at fixation while a task-irrelevant grating flickered in  
581 the background. Data from this task were used to compute an unbiased estimate of orientation  
582 selectivity for each voxel in visual areas V1-hV4v/V3A (see below).

583 We first examined whether category training increased the similarity of activation  
584 patterns evoked by exemplars from the same category (i.e., acquired similarity). We tested this  
585 by training a linear decoder (support vector machine) to discriminate between activation patterns  
586 associated with exemplars at the center of each category (48° from the boundary), then used the  
587 trained classifier to predict the category membership of exemplars immediately adjacent to the

588 category boundary ( $\pm 12^\circ$ ; Figure 2A). This analysis was performed separately for the orientation  
589 mapping and category discrimination tasks. We reasoned that if category training homogenizes  
590 activation patterns evoked by members of the same category, then decoding performance should  
591 be superior during the category discrimination task relative to the orientation mapping task. This  
592 is precisely what we observed (Figure 2B). For example, near-boundary decoding performance  
593 in V1 was reliably above chance during the category discrimination task ( $p < 0.0001$ , false-  
594 discovery-rate-corrected bootstrap test), but not during the orientation mapping task when the  
595 category boundary was irrelevant and the oriented stimulus was unattended ( $p = 0.38$ ).  
596 Importantly, the absence of robust decoding performance during the orientation mapping task  
597 cannot be attributed to poor signal, as a decoder trained and tested on activation patterns  
598 associated with exemplars at the center of each category (Figure 2C) yielded above-chance  
599 decoding during both behavioral tasks (Figure 2D;  $M = 0.58$  and  $0.69$  for the mapping and  
600 discrimination tasks, respectively;  $p < 0.01$ , bootstrap test). Collectively, these results suggest  
601 that category training can alter population-level responses at very early stages of the visual  
602 processing hierarchy.

603         To better understand how category training influences orientation-selective activation  
604 patterns in early visual cortical areas, we used an inverted encoding model (Brouwer & Heeger,  
605 2011) to generate model-based reconstructed representations of stimulus orientation from these  
606 patterns. For each visual area (e.g., V1), we first modelled voxel-wise responses measured during  
607 the orientation mapping task as a weighted sum of idealized orientation channels, yielding a set  
608 of weights that characterize the orientation selectivity of each voxel (Figure 3A). In the second  
609 phase of the analysis, we reconstructed trial-by-trial representations of stimulus orientation by  
610 combining these weights with the observed pattern of activation across voxels measured during

611 each trial of the category discrimination task, resulting in single-trial reconstructed channel  
612 response function that contains a representation of stimulus orientation for each ROI on each trial  
613 (Figure 3B). Finally, we sorted trial-by-trial reconstructions according to category membership  
614 such that any bias would manifest as a clockwise (rightward) shift of the orientation  
615 representation towards the center of Category 2 and quantified biases towards this category using  
616 a curve-fitting analysis (Methods).

617 Note that stimulus orientation was irrelevant during the orientation mapping task used for  
618 model weight estimation. We therefore reasoned that voxel-by-voxel responses evoked by each  
619 oriented stimulus would be largely uncontaminated by its category membership. Indeed, the  
620 logic of our analytical approach rests on the assumption that orientation-selective responses are  
621 quantitatively different during the orientation mapping and category discrimination tasks: if  
622 identical category biases are present in both tasks then the orientation weights computed using  
623 data from either task will capture that bias and reconstructed representations of orientation will  
624 not exhibit any category shift. This is precisely what we observed when we used a cross-  
625 validation approach to reconstruct stimulus representations separately for the orientation  
626 mapping and category discrimination tasks (Figure 4).

627 As shown in Figure 5, reconstructed representations of orientation in visual areas V1, V2,  
628 and V3 were systematically biased away from physical stimulus orientation and towards the  
629 center of the appropriate category (shifts of 22.13°, 26.65°, and 34.57°, respectively;  $P < 0.05$ ,  
630 bootstrap test, false-discovery-rate [FDR] corrected for multiple comparisons across regions; see  
631 Figure 6 for separate reconstructions of Category 1 and Category 2 orientations and Figure 7 for  
632 participant-by-participant reconstructions plotted by visual area). Similar, though less robust  
633 biases were also evident in hV4v and V3A (mean shifts of 9.73° and 6.45°, respectively;  $p >$

634 0.19). A logistic regression analysis established that categorical biases in V1-V3 were strongly  
635 correlated with variability in overt category judgments (Figure 8). That is, trial-by-trial category  
636 judgments were more strongly associated with the responses of orientation channels near the  
637 center of each category rather than those near the physical orientation of the stimulus.  
638 Importantly, because the location of the boundary separating categories 1 and 2 was randomly  
639 selected for each participant, it is unlikely that categorical biases shown in Figure 5 reflect  
640 intrinsic biases in stimulus selectivity in early visual areas (e.g., due to oblique effects; Sun et al.,  
641 2013).

642       The category biases shown in Figure 5 may be the result of an adaptive process that  
643 facilitates task performance by enhancing the discriminability of physically similar but  
644 categorically distinct stimuli. Consider a hypothetical example where an observer is tasked with  
645 discriminating between two physically similar exemplars on opposite sides of a category  
646 boundary. Discriminating between these alternatives should be challenging as each exemplar  
647 evokes a similar and highly overlapping response pattern. However, discrimination performance  
648 could be improved if the responses associated with each exemplar are made more separable via  
649 acquired distinctiveness following training (or equivalently, an acquired similarity between  
650 exemplars adjacent to the category boundary and exemplars near the center of each category).  
651 Similar changes would be less helpful when an observer is tasked with discriminating between  
652 physically and categorically distinct exemplars, as each exemplar already evokes a dissimilar and  
653 non-overlapping response. From these examples, a simple prediction can be derived: categorical  
654 biases in reconstructed representations of orientation should be largest when participants are  
655 shown exemplars adjacent to the category boundary and progressively weaker when participants  
656 are shown exemplars further away from the category boundary.

657 We tested this possibility by sorting stimulus reconstructions according to the angular  
658 distance between stimulus orientation and the category boundary (Figure 9). As predicted,  
659 reconstructed representations of orientations adjacent to the category boundary were strongly  
660 biased by category membership, with larger biases for exemplars nearest to the category  
661 boundary ( $\mu = 42.62^\circ$ ,  $24.16^\circ$ , and  $20.12^\circ$  for exemplars located  $12^\circ$ ,  $24^\circ$ , and  $36^\circ$  from the  
662 category boundary, respectively; FDR-corrected bootstrap  $p < 0.0015$ ), while reconstructed  
663 representations of orientations at the center of each category exhibited no signs of bias ( $\mu = -$   
664  $3.98^\circ$ ,  $p = 0.79$ ; the direct comparison of biases for exemplars adjacent to the category boundary  
665 and in the center of each category was also significant;  $p < 0.01$ ). Moreover, the relationship  
666 between average category bias and distance from the category boundary was well-approximated  
667 by a linear trend (slope =  $-14.38^\circ/\text{step}$ ;  $r^2 = 0.96$ ). Thus, category biases in reconstructed  
668 representation are largest under conditions where they would facilitate behavioral performance  
669 and absent under conditions where they would not.

670 Category-selective signals have been identified in multiple brain areas, including portions  
671 of lateral occipital cortex, inferotemporal cortex, posterior parietal cortex, and lateral prefrontal  
672 cortex (Sigala & Logothetis, 2002; Freedman et al., 2011; Freedman & Assad, 2006; Folstein et  
673 al., 2012; Davis & Poldrack, 2013; Pourtois et al., 2008; Mack et al., 2013). We identified  
674 category selective information in many of these same regions using a whole-brain searchlight-  
675 based decoding analysis where a classifier was trained to discriminate between exemplars from  
676 Category 1 and Category 2 (independently of stimulus orientation; Figure 10 and Methods).  
677 Next, we used the same inverted encoding model described above to reconstruct representations  
678 of stimulus orientation from activation patterns measured in each area during each of the  
679 orientation mapping and category discrimination tasks (reconstructions were computed using a



680 “leave-one-participant-out” cross-validation routine to ensure that reconstructions were  
681 independent of the decoding analysis used to define category-selective ROIs). We were able to  
682 reconstruct representations of stimulus orientation in many of these regions during the category  
683 discrimination task, but not during the orientation mapping task (where stimulus orientation was  
684 task-irrelevant; Figure 11). This is perhaps unsurprising as representations in many mid-to-high  
685 order cortical areas are strongly task-dependent (e.g., Silver et al., 2005). As our analytical  
686 approach requires an independent and unbiased estimate of each voxel’s orientation selectivity  
687 (e.g., during the orientation mapping task), this meant that we were unable to probe categorical  
688 biases in reconstructed representations in these regions.

#### 689 *Experiment 2 - EEG*

690       Due to the sluggish nature of the hemodynamic response, the category biases shown in  
691 Figures 5 and 9 could reflect processes related to decision making or response selection rather  
692 than stimulus processing. In a second experiment, we evaluated the temporal dynamics of  
693 category biases using EEG. Specifically, we reasoned that if the biases shown in Figures 5 and 9  
694 reflect processes related to decision making, response selection, or motor planning, then these  
695 biases should manifest only during a period shortly before the participants’ response.  
696 Conversely, if the biases are due to changes in how sensory neural populations encode features,  
697 they should be evident during the early portion of each trial. To evaluate these alternatives, we  
698 recorded EEG while a new group of 28 volunteers performed variants of the orientation mapping  
699 and categorization tasks used in the fMRI experiment. On each trial, participants were shown a  
700 large annulus of iso-oriented bars that flickered at 30 Hz (i.e., 16.67 ms on, 16.67 ms off; Figure  
701 12A). During the orientation mapping task, participants detected and reported the identity of a  
702 target letter (an X or a Y) that appeared in a rapid series of letters over the fixation point.

703 Identical displays were used during the category discrimination task, with the caveat that  
704 participants were asked to report the category of the oriented stimulus while ignoring the letter  
705 stream.

706         The 30 Hz flicker of the oriented stimulus elicits a standing wave of frequency-specific  
707 sensory activity known as a steady-state visually-evoked potential (SSVEP, Vialatte et al., 2010;  
708 Figure 12B). The coarse spatial resolution of EEG precludes precise statements about the cortical  
709 source(s) of these signals (e.g., V1, V2, etc.). However, to focus on visual areas (rather than  
710 parietal or frontal areas) we deliberately entrained stimulus-locked activity at a relatively high  
711 frequency (30 Hz). Our approach was based on the logic that coupled oscillators can only be  
712 entrained at high frequencies within small local networks, while larger or more distributed  
713 networks can only be entrained at lower frequencies due to conduction delays (Breakspear et al.,  
714 2010). Indeed, a topographic analysis showed that evoked 30 Hz activity was strongest over a  
715 localized region of occipitoparietal electrode sites. (Figure 12C). As in Experiment 1,  
716 participants learned to categorize stimuli with a high degree of accuracy, with errors and slow  
717 responses present only for exemplars adjacent to a category boundary (Figure 12D-E)

718         We computed the power and phase of the 30 Hz SSVEP response across each 3,000 ms  
719 trial and then used these values to reconstruct a time-resolved representation of stimulus  
720 orientation (Garcia et al., 2013). Our analysis procedure followed that used in Experiment 1: In  
721 the first phase of the analysis, we rank-ordered scalp electrodes by 30 Hz power (based on a  
722 discrete Fourier transform spanning the 3000 ms trial epoch, averaged across all trials of both the  
723 orientation mapping and category discrimination tasks). Responses measured during the  
724 orientation mapping task were used to estimate a set of orientation weights for the 32 electrodes  
725 with the strongest SSVEP signals (i.e., those with the highest 30 Hz power; see Figure 12C) at

726 each timepoint. In the second phase of the analysis, we used these timepoint-specific weights and  
727 corresponding responses measured during each trial of the category discrimination task across all  
728 electrodes to compute a time-resolved representation of stimulus orientation (Figure 13A-B). We  
729 reasoned that if the categorical biases shown in Figures 5 and 9 reflect processes related to  
730 decision making or response selection, then they should emerge gradually over the course of  
731 each trial. Conversely, if the categorical biases reflect changes in sensory processing, then they  
732 should manifest shortly after stimulus onset. To test this possibility, we computed a temporally  
733 averaged stimulus reconstruction over an interval spanning 0 to 250 ms after stimulus onset  
734 (Figure 14B). A robust category bias was observed ( $M = 23.35^\circ$ ;  $p = 0.014$ ; bootstrap test)  
735 suggesting that the intent to categorize a stimulus modulates how neural populations in early  
736 visual areas respond to incoming sensory signals.

737       Importantly, the bandpass filter used to isolate 30 Hz activity will distort temporal  
738 characteristics of the raw EEG signal by some amount. We estimated the extent of this distortion  
739 by generating a 3 second, 30 Hz sinusoid with unit amplitude (plus 1 second of pre- and post-  
740 signal zero padding) and running it through the same filters used in our analysis path. We then  
741 computed the time at which the filtered signal reach 25% of maximum. For an instantaneous  
742 filter, this should occur at exactly 1 second (due to the pre- and post-signal zero-padding). We  
743 estimated a signal onset of  $\sim 877$  ms, or 123 ms prior to the start of the signal. Therefore, if  
744 reconstruction amplitude is greater than zero at time  $t$ , then we can conclude that the pattern of  
745 scalp activity used to generate the stimulus reconstruction contained reliable orientation  
746 information at time  $t \pm 125$  ms. The same logic applies to estimates of reconstruction bias as the  
747 reconstructions are based on data filtered using the same parameters. Importantly, we also  
748 verified that there was no categorical bias in stimulus reconstructions prior to stimulus onset

749 (Figure 14), nor were categorical biases present when we reconstructed stimulus representations  
750 using data from the orientation mapping and category discrimination tasks separately (Figure  
751 15).

752 *Ruling out contributions from eye movements.* We identified and removed trials contaminated by  
753 large EOG artifacts (blinks and eye movements greater than  $\sim 2^\circ$ ). However, small and consistent  
754 eye movement patterns could nevertheless contribute to the orientation reconstructions reported  
755 here. We examined this possibility by testing whether participants foveated the inner aperture of  
756 the stimulus at polar locations matching its orientation (Figure 16A) or at polar locations  
757 matching the center of the appropriate category (A vs B; Figure 16B; see Methods for details).  
758 No systematic differences in eye position were observed as a function of stimulus orientation or  
759 category membership (Figure 16), suggesting that eye movements were not a major contributor  
760 to orientation-specific reconstructions.

### 761 *Experiment 3 - EEG*

762 The results of Experiments 1 and 2 suggest that category learning can bias stimulus-  
763 specific representations encoded by occipitoparietal cortical areas. However, an alternative  
764 explanation is that the biases shown in Figures 5, 9, and 13 reflect mechanisms of response  
765 selection or decision making independent of categorical processing. Experiment 3 examined this  
766 possibility by examining categorical biases in stimulus-specific memory representations while  
767 participants performed a delayed match-to-category (DMC) task. A schematic of the task is  
768 shown in Figure 17A-B. At the beginning of each trial a sample disc rendered in one of 12  
769 possible stimulus locations ( $15\text{-}345^\circ$  polar angle in  $30^\circ$  along the perimeter of an imaginary  
770 circle). Half of the disc positions were assigned membership in Category 1, while the remaining  
771 half of disc positions were assigned membership in Category 2 (Figure 17A). Participants

772 remembered the position of the sample disc over a blank delay, then judged whether a probe disc  
773 was rendered in a position matching the category of the sample disc. The location of the category  
774 boundary was randomly determined for each participant, and response feedback (correct vs.  
775 incorrect) was provided after every trial. Like Experiment 2, participants were not trained on the  
776 DMC task prior to testing and learned to associate specific positions with specific categories  
777 through feedback. Before completing the DMC task, participants also completed a spatial  
778 working memory task. Display and stimulus geometry were identical during the spatial memory  
779 task and the DMC task. On each trial a sample disc was rendered in one of the same 12 positions  
780 used during the DMC task. After a short delay, participants recalled the location of the sample  
781 disc via mouse click.

782       Following earlier work (e.g., Foster et al., 2016; Samaha et al., 2016; Ester et al., 2018;  
783 Nouri & Ester, 2019), we used spatiotemporal patterns of induced alpha-band (8-12 Hz) activity  
784 over occipitoparietal electrode sites to track the contents of spatial working memory during the  
785 recall and DMC tasks. Specifically, we modeled sample-by-sample estimates of alpha band  
786 activity recorded during the spatial recall task as a combination of 12 location filters, each with  
787 an idealized tuning curve (a cosine raised to the 12<sup>th</sup> power). The result of this step is a set of  
788 weights that characterizes the location preferences of each scalp electrode. Next, we used these  
789 weights and spatiotemporal patterns of alpha-band activity recorded during the DMC task to  
790 compute an expected response for each location filter, yielding a time-resolved estimate of  
791 stimulus position. Trial-by-trial response functions were shifted to a common center (0° by  
792 convention), averaged, and arranged such that any category bias would manifest as a clockwise  
793 or positive shift towards the center of Category 2.

794 As expected, a robust category bias was observed during the delay period of the DMC  
795 task (Figure 17C), though unlike Experiment 2 the bias seemed to emerge gradually over the  
796 course of the delay period. To quantify this bias, we averaged channel responses from period  
797 0.25 to 2.0 sec after onset of the sample display and fit the resulting function with an  
798 exponentiated cosine (*Quantification of Bias in Orientation Representations*, Methods). Mean  
799 reconstruction centers were reliably greater than  $0^\circ$  ( $M = 10.55^\circ$ ;  $p = 0.002$ , bootstrap test),  
800 indicating a robust bias towards the center of the relevant category. Importantly, this bias cannot  
801 be explained by mechanisms associated with decision making and response selection:  
802 participants could not plan or implement a response until the probe stimulus was presented at the  
803 end of the delay period. This result further suggests that the results of Experiments 1 and 2  
804 cannot be wholly explained by mechanisms of response selection or bias.

805 *Assessing contributions from eye movements.* We identified and removed electrooculogram  
806 artifacts from the data via independent components analysis. However, small and consistent eye  
807 movement patterns opaque to ICA could nevertheless contribute to the location reconstructions  
808 reported here. We examined this possibility by regressing time-resolved estimates of horizontal  
809 EOG activity onto remembered stimulus locations. As shown in Figure 18, the regression  
810 coefficients linking eye position with remembered locations were indistinguishable from 0 for  
811 the duration of each trial, suggesting that eye movements were not a major determinant of  
812 location reconstructions.

813

**Discussion**

814 Our findings suggest that category learning shapes information processing at the earliest  
815 stages of the visual system. The results of Experiment 1 showed that representations of a to-be-  
816 categorized stimulus encoded by population-level activity in early visual cortical areas were  
817 systematically biased by their category membership. These biases were correlated with overt  
818 category judgments and were largest for exemplars adjacent to the category boundary. The  
819 results of Experiments 2 and 3 demonstrate that similar biases are present in orientation- and  
820 location-specific reconstructions computed by human scalp EEG data, and further suggest that  
821 our findings cannot be explained by response bias, motor planning, or eye movements.

822 The categorical biases reported here are strongly task dependent, and therefore must  
823 reflect changes in responses caused by transient top-down factors rather than long-term changes  
824 in feature or location selectivity. However, the effects of these top down modulations are  
825 fundamentally different from task-dependent modulations reported elsewhere. In one example,  
826 Ester et al. (2016) asked participants to attend the orientation or luminance of a peripheral  
827 grating and found both multiplicative and additive enhancements of orientation-specific  
828 reconstructions during the attend orientation condition relative to the attend luminance condition,  
829 but no evidence for a shift like the one reported here. In a different study, Byers and Serences  
830 (2014) examined changes in orientation-specific reconstructions before and after participants  
831 underwent extensive training (10 1-hour sessions) in a challenging orientation discrimination  
832 task. We observed changes in the amplitude (i.e., signal-to-noise ratio) of orientation-specific  
833 reconstructions following training, but no evidence for a shift like the one reported in the current  
834 study. In other studies, Scolari et al. (2012; 2014) examined changes in orientation-specific  
835 reconstructions when participants performed fine-grained and coarse-grained orientation

836 discrimination tasks. Participants viewed two oriented gratings in sequence and judged whether  
837 they were identical. During one experiment participants were cued to how the second grating  
838 might differ from the first (clockwise vs. counterclockwise rotation), while in a second  
839 experiment they were not. During the fine-grained discrimination task, the authors observed a  
840 modest shift in orientation-specific reconstructions towards “off-target” neural populations that  
841 maximally discriminated between two oriented stimuli, but only when participants were cued to  
842 expect a clockwise or counterclockwise rotation. While this type of modulation is desirable while  
843 performing a fine-discrimination task, it is qualitatively different than the shifts we report in the  
844 current experiment, as participants have no way of anticipating what orientation will be  
845 presented on each trial, nor the difference between that orientation and the category boundary.  
846 Moreover, the shifts reported by Scolari et al. (2012) during fine discriminations were relatively  
847 modest – at most few degrees. We report an opposite pattern of findings, where shifts are largest  
848 for oriented exemplars immediately adjacent to the category boundary. Thus, while other studies  
849 have documented task-dependent changes in orientation-specific reconstructions, those studies  
850 have failed to reveal shifts in reconstructed representations (Ester et al., 2016; Byers & Serences  
851 2014) or have revealed modest shifts that follow different patterns from those reported here  
852 (Scolari et al. 2012).

853         Several mechanisms may be responsible for our findings. One possibility is that the  
854 orientation preferences of single-units (or populations of units) are systematically shifted towards  
855 the center of each category during the category discrimination task, much in the same way that  
856 neurons in the rodent auditory system exhibit emergent selectivity for categorically different  
857 stimuli (e.g., Xin et al., 2019) or in the same way that the spectral preferences of neural  
858 populations are biased by feature-based attention (David et al., 2008; Cukur et al., 2012). These



859 shifts are relatively small at the single unit level but could be amplified by a read-out  
860 mechanisms that integrate the responses of large neural populations. A second possibility is that  
861 participants strategically apply gain to neural populations that maximally discriminate between  
862 to-be-categorized exemplars during the category discrimination task. Here there are no changes  
863 in the spectral preferences of single units, but the responses of neurons that respond to stimuli  
864 near the category boundary are amplified. These alternatives are not mutually exclusive; nor is  
865 this an exhaustive list. Our data cannot resolve these possibilities. For example, several different  
866 patterns of single-unit gain changes and/or tuning shifts can produce identical responses in a  
867 single fMRI voxel, and different patterns of single-voxel modulation could produce categorical  
868 biases in multivariate stimulus reconstructions (see, e.g., Sprague et al., 2018 for a detailed  
869 discussion of this issue). Ultimately, targeted experiments that combine non-invasive  
870 measurements of brain activity with careful psychophysical measurements and detailed model  
871 simulations will be needed to conclusively identify the mechanisms responsible for the category  
872 biases we have reported here.

873         Our findings appear to conflict with results from nonhuman primate research which  
874 suggests that sensory cortical areas do not encode categorical information. However, there is  
875 reason to suspect that mechanisms of category learning might be qualitatively different in human  
876 and non-human primates. For example, our participants learned to categorize stimuli based on  
877 performance feedback after approximately 10 minutes of training. In contrast, macaque monkeys  
878 typically require six months or more of training using a similar feedback scheme to reach a  
879 similar level of performance, and this extensive amount of training may influence how neural  
880 circuits code information (e.g., Itthipuripat et al., 2017; Birman & Gardner, 2015). Moreover,  
881 there is growing recognition that the contribution(s) of sensory cortical areas to performance on a

882 visual task are highly susceptible to recent history and training effects (Itthipurripiat et al., 2017,  
883 Chen et al., 2016; Liu & Pack, 2017). In one example (Liu & Pack, 2017), extensive training was  
884 associated with a functional substitution of human visual area V3a for MT+ in discriminating  
885 noisy motion patches. Thus, training effects may help explain why previous electrophysiological  
886 experiments have found category-selective responses in association but not sensory cortical  
887 areas.

888         Studies of categorization in non-human primates have typically employed variants of a  
889 delayed match to category task, where monkeys are shown a sequence of two exemplars  
890 separated by a blank delay interval and asked to report whether the category of the second  
891 exemplar matches the category of the first exemplar. The advantage of this task is that it allows  
892 experimenters to decouple category-selective signals from activity related to decision making,  
893 response preparation, and response execution. However, this same advantage also precludes  
894 examinations of whether and/or how top-down category-selective signals interact with bottom-up  
895 stimulus-specific signals. We made no effort to decouple category-selective and decision-related  
896 signals in Experiments 1-2, and thus the category biases observed in those studies could reflect  
897 mechanisms of decision making, response selection, or motor planning. The results of  
898 Experiment 3 conflict with this interpretation by demonstrating that robust category biases are  
899 present during the memory period of a delayed match-to-category task (Freedman & Assad,  
900 2006).

901         Previous studies have identified cortical modules selective for faces (Kanwisher et al.,  
902 1997), locations (Epstein & Kanwisher, 1998), actions (Astafiev et al., 2004; Huth et al., 2012),  
903 bodies (Downing et al., 2001); animacy (Konkle & Caramazza, 2013) and size (Konkle &  
904 Caramazza, 2013). Other category distinctions (e.g., tools vs. cars) lack specialized processing

905 modules but can be decoded from multivoxel patterns in multiple occipitotemporal regions (e.g.,  
906 Folstein et al., 2012). Our findings complement these studies by demonstrating that learning a  
907 novel and arbitrary category rule is correlated with rapid and reversible changes in stimulus-  
908 specific information processing at even earlier stages of the cortical visual processing hierarchy,  
909 including V1 (see also Brouwer & Heeger, 2009; 2013). Category-dependent changes in early  
910 visual areas may contribute to more complex forms of category selectivity exhibited by upstream  
911 cortical areas, including portions of lateral occipital and inferotemporal cortex. This possibility  
912 awaits further scrutiny.

913       To summarize, we have shown that learning a novel and arbitrary category rule based on  
914 a simple visual feature (orientation or location) correlates with rapid and reversible changes in  
915 sensory and mnemonic representations encoded by regions in early occipitoparietal cortex. These  
916 changes correlate with participants' overt category judgments, are largest for exemplars adjacent  
917 to a category boundary, and cannot be explained by decision making or motor preparation.  
918 Collectively, these results provide novel and important evidence suggesting that category  
919 learning induces rapid-yet-reversible changes in information processing at early stages of the  
920 cortical visual processing hierarchy.

921

## References

- 922
- 923 Ashby FG, Maddox WT (2005) Human category learning. *Annu Rev Psychol* 56:148-178.
- 924 Astafiev SV, Stanley CM, Shulman GL, Corbetta M (2004) Extrastriate body area in human  
925 occipital cortex responds to the performance of motor actions. *Nat Neurosci* 7:542-548
- 926 Birman D, Gardiner JL (2015) Parietal and prefrontal: categorical differences? *Nat Neurosci*  
927 19:5-7
- 928 Breakspear M, Heitmann S, Daffertshofer A (2010) Generative models of cortical oscillations:  
929 Neurobiological implication of the Kuramoto model. *Front Hum Neurosci* 4:190
- 930 Brouwer GJ, Heeger DJ (2011) Decoding and reconstructing color from responses in human  
931 visual cortex. *J Neurosci* 29:13992-14003
- 932 Brouwer GJ, Heeger DJ (2011) Cross-orientation suppression in human visual cortex. *J*  
933 *Neurophysiol* 106:2108-2119.
- 934 Brouwer GJ, Heeger DJ (2013) Categorical clustering of the neural representation of color. *J*  
935 *Neurosci* 33:15454-15465
- 936 Byers A, Serences JT (2014) Enhanced attentional gain as a mechanism for generalized  
937 perceptual learning in human visual cortex. *J Neurophysiol* 112:1217-1227
- 938 Chang C-C, Lin CJ (2011) LIBSVM: A library for support vector machines. *ACM Trans Intell*  
939 *Syst Technol* 2(27):1-27
- 940 Chen N, Cai P, Zhou T, Thompson B, Fang F (2016) Perceptual learning modifies the functional  
941 specializations of visual cortical areas. *Proc Natl Acad Sci USA* 113:5724-5729
- 942 Cousineau D (2005) Confidence intervals in within-subject designs: A simpler solution to Loftus  
943 & Masson's method. *Quant Meth Psych* 1:42-45

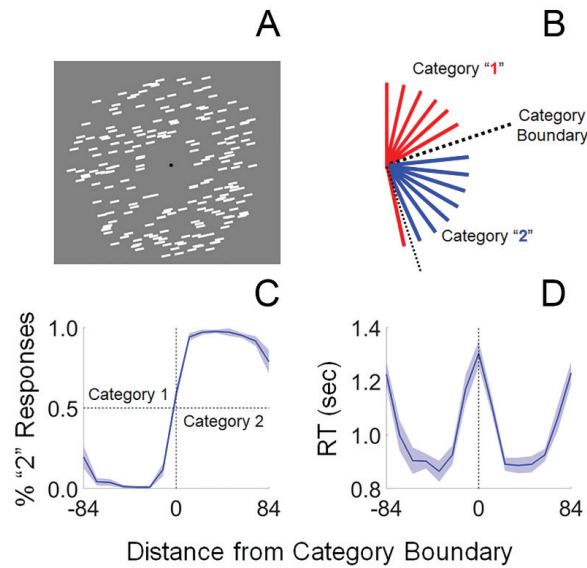
- 944 Cukur T, Nishimoto S, Huth AG, Gallant JL (2013) Attention during natural vision warps  
945 semantic representation across the human brain. *Nat Neurosci* 16:763-770
- 946 David SV, Hayden BY, Mazer JA, Gallant JL (2008) Attention to stimulus features shifts  
947 spectral tuning of V4 neurons during natural vision. *Neuron* 59:509-521
- 948 Davis T, Poldrack RA (2013) Quantifying the internal structure of categories using a neural  
949 typicality measure. *Cereb Cortex* 24:1720-1737.
- 950 Downing PE, Jiang Y, Shuman M, Kanwisher N (2001) A cortical area selective for visual  
951 processing of the human body. *Science* 293:2470-2473
- 952 Epstein R, Kanwisher N (1998) A cortical representation of the local visual environment. *Nature*  
953 392:598
- 954 Ester EF, Sprague TC, Serences JT (2015) Parietal and frontal cortex encode stimulus-specific  
955 mnemonic representations during visual working memory. *Neuron* 87:893-905.
- 956 Ester EF, Nouri A, Rodriguez L (2018) Retrospective cues mitigate information loss in human  
957 cortex during working memory storage. *J Neurosci* 38:8538-8548
- 958 Esterman M, Tamber-Rosenau BJ, Chiu Y-C, Yantis S (2010) Avoiding non-independence in  
959 fMRI data analysis: Leave one subject out. *NeuroImage* 50:572-576
- 960 Folstein JR, Palmeri TJ, Gauthier I (2012) Category learning increases discriminability of  
961 relevant object dimensions in visual cortex. *Cereb Cortex* 23:714-823.
- 962 Freedman DJ, Riesenhuber M, Poggio T, Miller EK (2011) Categorical representation of visual  
963 stimuli in the primate prefrontal cortex. *Science* 291:312-316
- 964 Freedman DJ, Assad JA (2006) Experience-dependent representation of visual categories in  
965 parietal cortex. *Nature* 443:85-88.

- 966 Friston K (2010) The free-energy principle: A unified brain theory? *Nat Rev Neurosci* 11:127-  
967 138
- 968 Garcia JO, Sreenivasan R, Serences JT (2013) Near-real-time feature-selective modulations in  
969 human cortex. *Curr Biol* 23:515-522
- 970 Gardiner JL, Liu T (2019) Inverted encoding models reconstruct an arbitrary model response, not  
971 the stimulus. *eNeuro*
- 972 Goldstone RL (1994) Influence of categorization on perceptual discrimination. *J Exp Psychol*  
973 *Gen* 123:178-200
- 974 Goldstone RL (1998) Perceptual Learning. *Annu Rev Psychol* 49:585-612
- 975 Huth AG, Nishimoto S, Vu AT, Gallant JL (2012) A continuous semantic space describes the  
976 representation of thousands of object and action categories across the human brain.  
977 *Neuron* 76:1210-1224
- 978 Itthipuripat S, Cha K, Byers A, Serences JT (2017) Two different mechanisms support selective  
979 attention at different phases of training. *PLOS Biology*
- 980 Jazayeri M, Movshon JA (2006) Optimal representation of sensory information by neural  
981 populations. *Nat Neurosci* 9:690-696
- 982 Kanwisher N, McDermott J, Chun MM (1997) The fusiform face area: a module in human  
983 extrastriate cortex specialized for face perception. *J Neurosci* 17:4302-4311
- 984 Konkle T, Caramazza A (2013) Tripartite organization of the ventral stream by animacy and  
985 object size. *J Neurosci* 33:10235-10242
- 986 Kleiner M, Brainard D, Pelli D (2007) What's new in Psychtoolbox-3. *Perception* 36(14)
- 987 Koida K, Komatsu H (2007) Effects of task demands on the responses of color-selective neurons  
988 in the inferior temporal cortex. *Nat Neurosci* 10:108-116

- 989 Liu LD, Pack CC (2017) The contribution of area MT to visual motion perception depends on  
990 training. *Neuron* 95:436-446
- 991 Livingston K, Andrews J, Harnad S (1998) Categorical perception effects induced by category  
992 learning. *J Exp Psychol Learn Mem Cogn* 24:732-753.
- 993 Mack ML, Preston AR, Love BC (2013) Decoding the brain's algorithm for categorization from  
994 its neural implementation. *Curr Biol* 23:2023-2027.
- 995 Martinez-Trujillo JC, Treue S (2004) Feature-based attention increases the selectivity of  
996 population responses in primate visual cortex. *Curr Biol* 14:744-751.
- 997 Navalpakkam V, Itti L (2007) Search goal tunes visual features optimally. *Neuron* 53:605-617
- 998 Newell FN, Bulthoff HH (2002) Categorical perception of familiar objects. *Cognition* 85:113-  
999 143
- 1000 Nouri A, Ester EF (2019) Recovery of information from latent memory stores decreases over  
1001 time. *Cogn Neurosci* doi: 10.1080/17588928.2019.1617258
- 1002 Pourtois G, Schwartz S, Spiridon M, Martuzzi R, Vuilleumier P (2008) Object representations  
1003 for multiple visual categories overlap in lateral occipital and medial fusiform cortex.  
1004 *Cereb Cortex* 19:1806-1819
- 1005 Rao RPN, Ballard DH (1999) Predictive coding in the visual cortex: A functional interpretation  
1006 of some extra-classical receptive-field effects. *Nat Neurosci* 2:79-87
- 1007 Scolari M, Serences JT (2010) Basing perceptual decision on the most informative sensory  
1008 neurons. *J Neurophysiol* 104:2266-2273
- 1009 Scolari M, Byers A, Serences JT (2012) Optimal deployment of attentional gain during fine  
1010 discriminations. *J Neurosci* 32:7723-7733

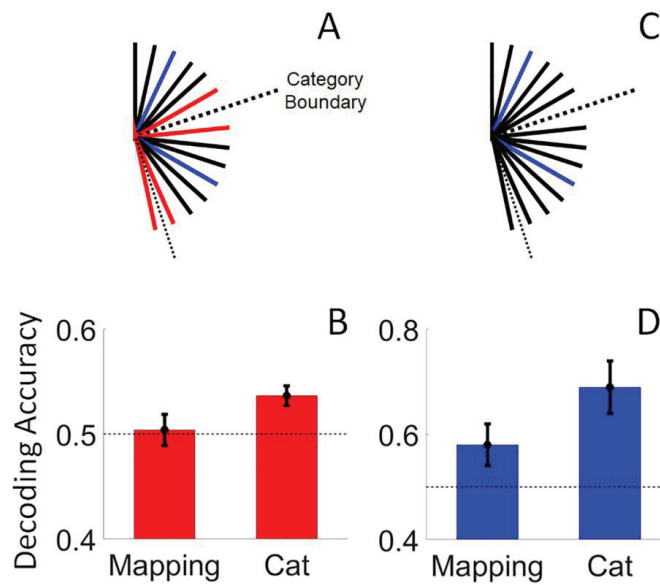
- 1011 Sigala N, Logothetis NK (2002) Visual categorization shapes feature selective in the primate  
1012 temporal cortex. *Nature* 415:318-320.
- 1013 Silver MA, Ress D, Heeger DJ (2005) Topographic maps of visual spatial attention in human  
1014 parietal cortex. *J Neurophysiol* 94:1358-1371
- 1015 Sprague TC, Adam KCS, Foster JJ, Rahmati M, Sutterer DW, Vo VA (2018) Inverted encoding  
1016 models assay population-level stimulus representations, not single-unit neural tuning.  
1017 *eNeuro* 5(3)
- 1018 Sun P, Gardiner JL, Costagli M, Ueno K, Waggoner RA, *et al.* Demonstration of tuning to  
1019 stimulus orientation in the human cortex: A high-resolution fMRI study with a novel  
1020 continuous stimulation paradigm. *Cereb Cortex* 23:1618-1629
- 1021 Viallatter F-B, Maurice M, Dauwels J, Cichocki A (2010) Steady-state visually evoked  
1022 potentials: Focus on essential paradigms and future perspectives. *Prog Neurobiol* 90:418-  
1023 438
- 1024





1025

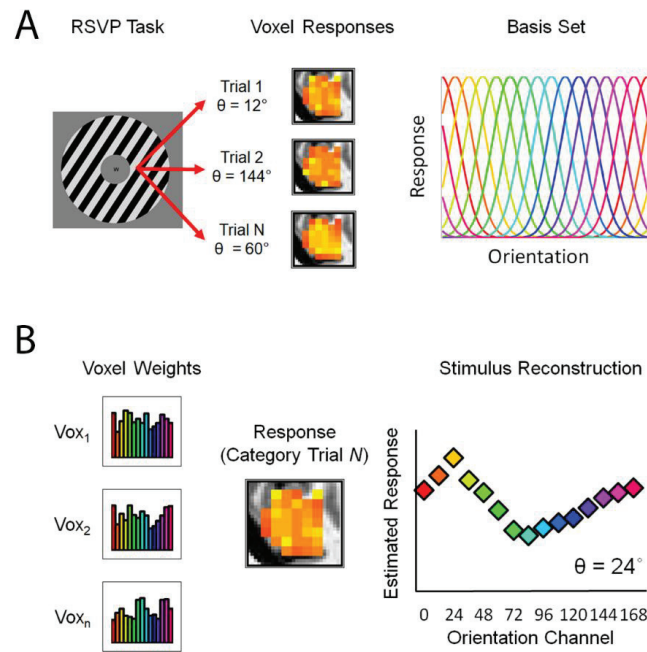
1026 **Figure 1. Overview of Experiment 1.** (A) Participants viewed displays containing a circular  
 1027 aperture of iso-oriented bars. On each trial, the bars were assigned one of 15 unique orientations  
 1028 from 0-168°. (B) We randomly selected and designated one stimulus orientation as a category  
 1029 boundary (black dashed line), such that the seven orientations counterclockwise from this value  
 1030 were assigned to Category 1 (red lines) and the seven orientations clockwise from this value  
 1031 were assigned to Category 2 (blue lines). (C) After training, participants rarely miscategorized  
 1032 orientations. (D) Response latencies are significantly longer for oriented exemplars near the  
 1033 category boundary (RT = response time; shaded regions in C-D are  $\pm 1$  within-participant  
 1034 S.E.M.).  
 1035



1036  
1037

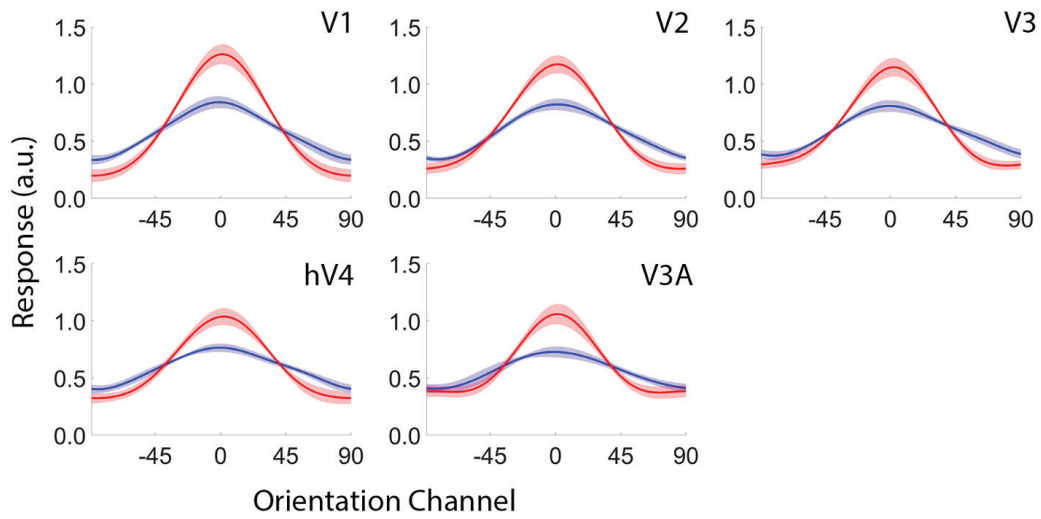
1038 **Figure 2. Category Decoding Performance.** (A) We trained classifiers on activation patterns  
1039 evoked by exemplars at the center of each category boundary during the orientation mapping and  
1040 category discrimination task (blue lines), then used the trained classifier to predict the category  
1041 membership of exemplars adjacent to the category boundary (red lines). (B) Decoding accuracy  
1042 was significantly higher during the category discrimination task relative to the orientation  
1043 mapping task ( $p = 0.01$ ), suggesting that activation patterns evoked by exemplars adjacent to the  
1044 category boundary became more similar to activation patterns evoked by exemplars at the center  
1045 of each category during the categorization task. The absence of robust decoding performance  
1046 during the orientation mapping task cannot be attributed to poor signal or a uniform enhancement  
1047 of orientation representations by attention, as a decoder trained and tested on activation patterns  
1048 associated with exemplars at the center of each category (C) yielded above-chance decoding  
1049 during both behavioral tasks (D). Decoding performance was computed from activation patterns  
1050 in V1. Error bars depict  $\pm 1$  S.E.M.

1051  
1052



1053  
 1054  
 1055  
 1056  
 1057  
 1058  
 1059  
 1060  
 1061  
 1062  
 1063  
 1064

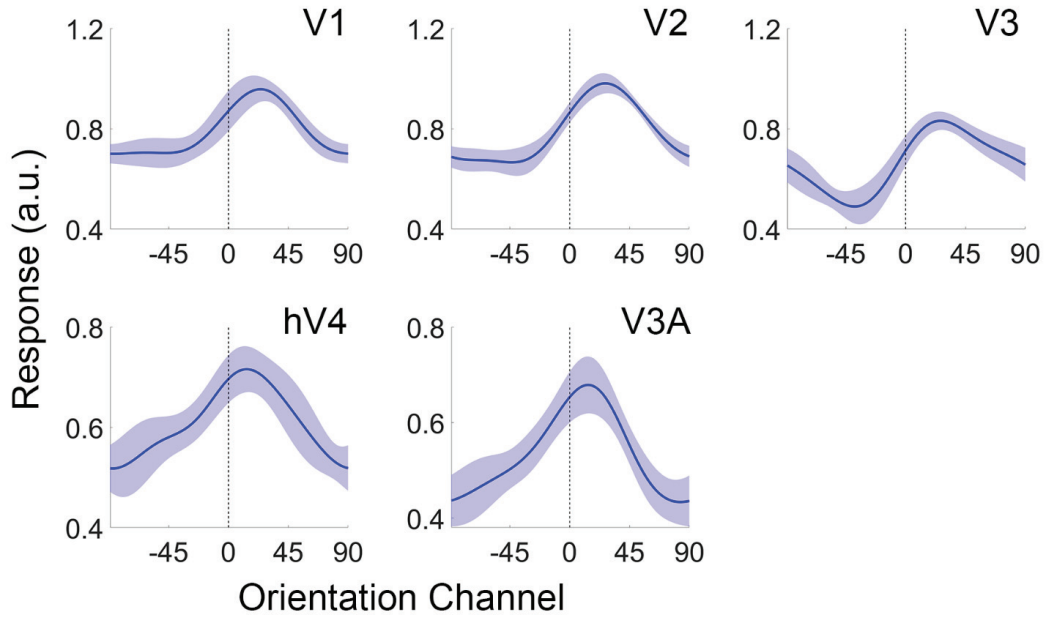
**Figure 3. Inverted Encoding Model.** (A) In the first phase of the analysis, we estimated an orientation selectivity profile for each voxel retinotopically organized V1-hV4/V3a using data from an independent orientation mapping task. Specifically, we modeled the response of each voxel as a set of 15 hypothetical orientation channels, each with an idealized response function. (B) In the second phase of the analysis, we computed the response of each orientation channel from the estimated orientation weights and the pattern of responses across voxels measured during each trial of the category discrimination task. The resulting reconstructed channel response function (CRF) contains a representation of the stimulus orientation (example; 24 deg), which we quantified via a curve-fitting procedure.



1065  
 1066  
 1067  
 1068  
 1069  
 1070  
 1071  
 1072  
 1073

**Figure 4. Reconstructions of stimulus orientation during the orientation mapping task (blue) and the category discrimination task (red).** Reconstructions were computed using a leave-one-run-out cross validation approach where data from N-1 runs were used to estimate channel weights and data from the remaining run were used to estimate channel responses. This procedure was iterated until all runs had been used to estimate channel responses and the results were averaged over permutations. No categorical biases were observed in any visual area for either task. Shaded regions depict  $\pm 1$  within-participant S.E.M. a.u., arbitrary units.

1074



1075

1076

1077

1078

1079

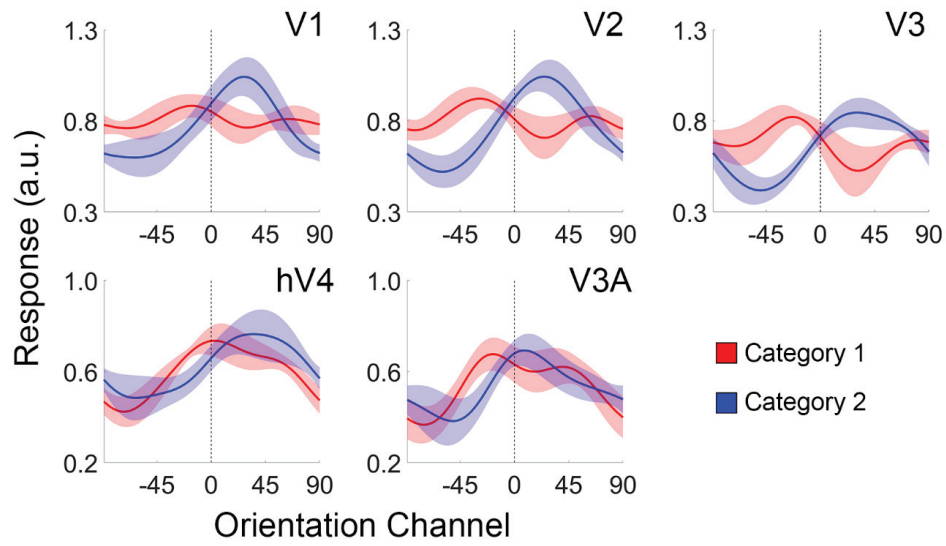
1080

1081

1082

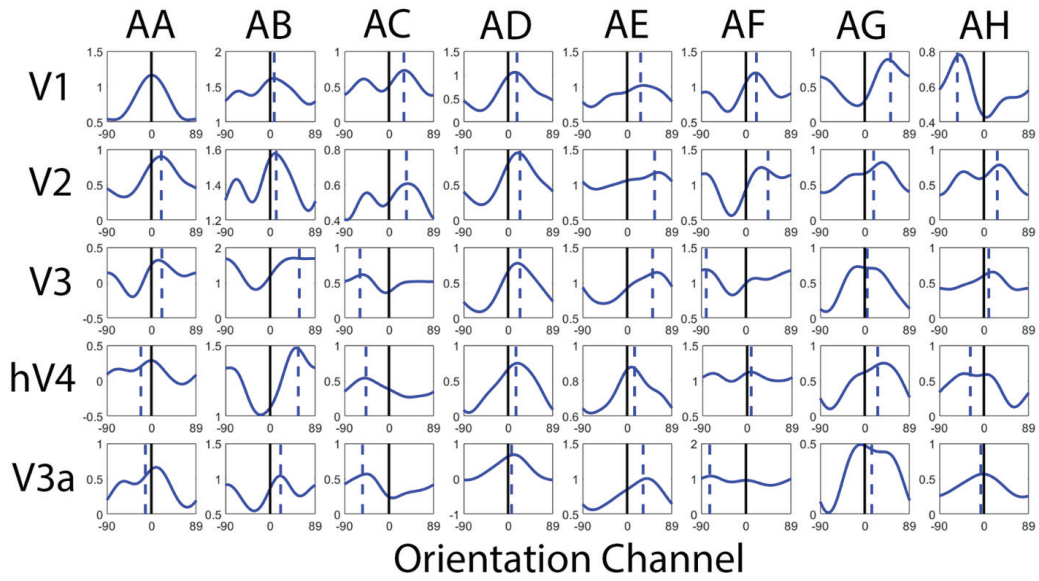
1083

**Figure 5. Reconstructed representations of Orientation in Early Visual Cortex.** The vertical bar at  $0^\circ$  indicates the actual stimulus orientation presented on each trial. Channel response functions (CRFs) from Category 1 and Category 2 trials have been arranged and averaged such that any categorical bias would manifest as a clockwise (rightward) shift in the orientation representation towards the center of Category B. Shaded regions are  $\pm 1$  within-participant S.E.M (see Methods). Note change in scale between visual areas V1-V3 and hV4-V3A. a.u., arbitrary units.



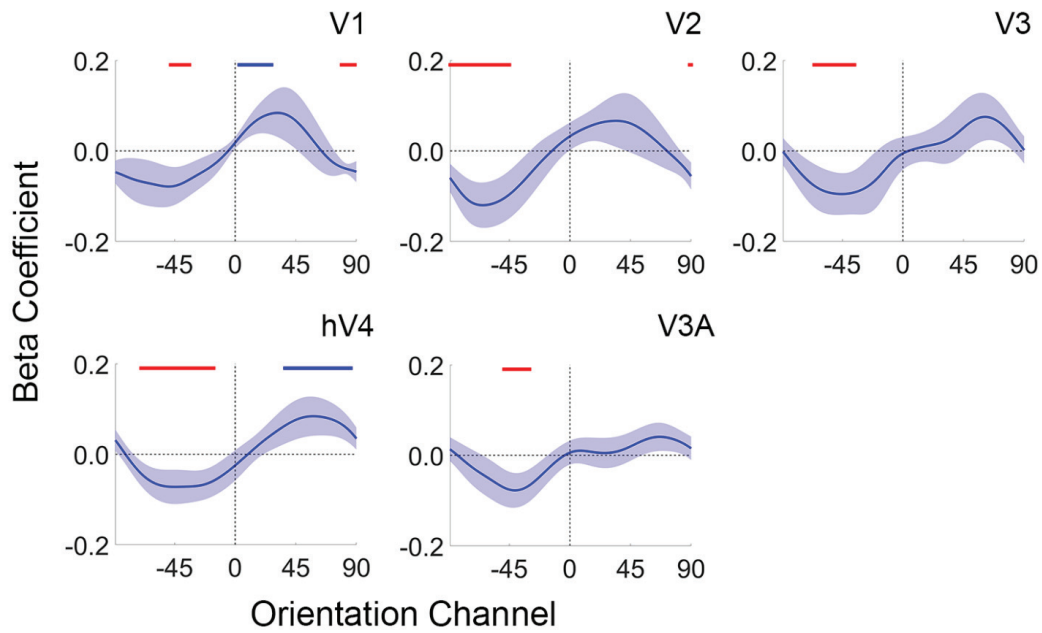
1084  
 1085  
 1086  
 1087  
 1088

**Figure 6. Stimulus Reconstructions during Category 1 and Category 2 trials.** Shaded regions are  $\pm 1$  within-participant S.E.M. a.u., arbitrary units.



1089  
 1090  
 1091  
 1092  
 1093  
 1094  
 1095

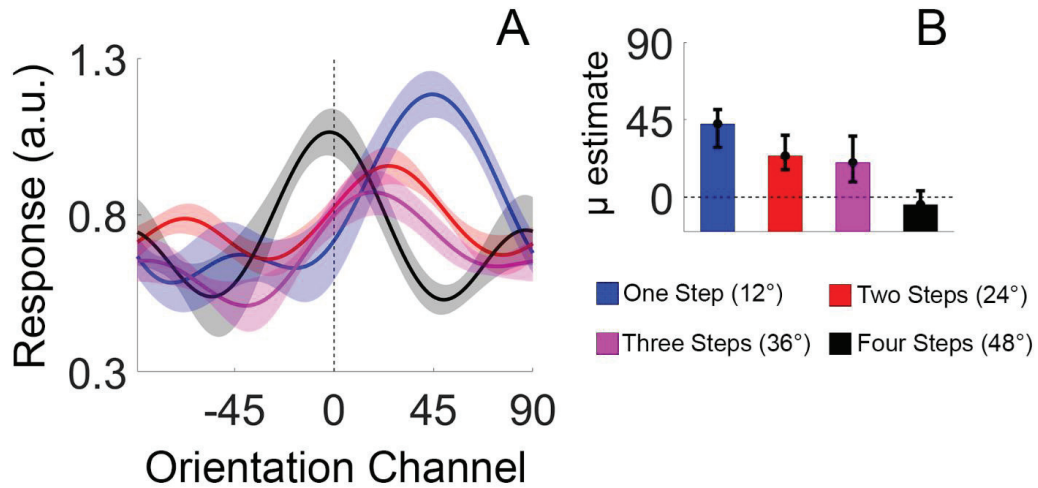
**Figure 7. Participant-level Stimulus Reconstructions.** Each panel plots a reconstructed representation of stimulus orientation for a given participant (columns) and visual area (rows). Dashed blue lines are the estimated peak of each reconstruction (obtained via curve-fitting). Ordinate units are arbitrary.



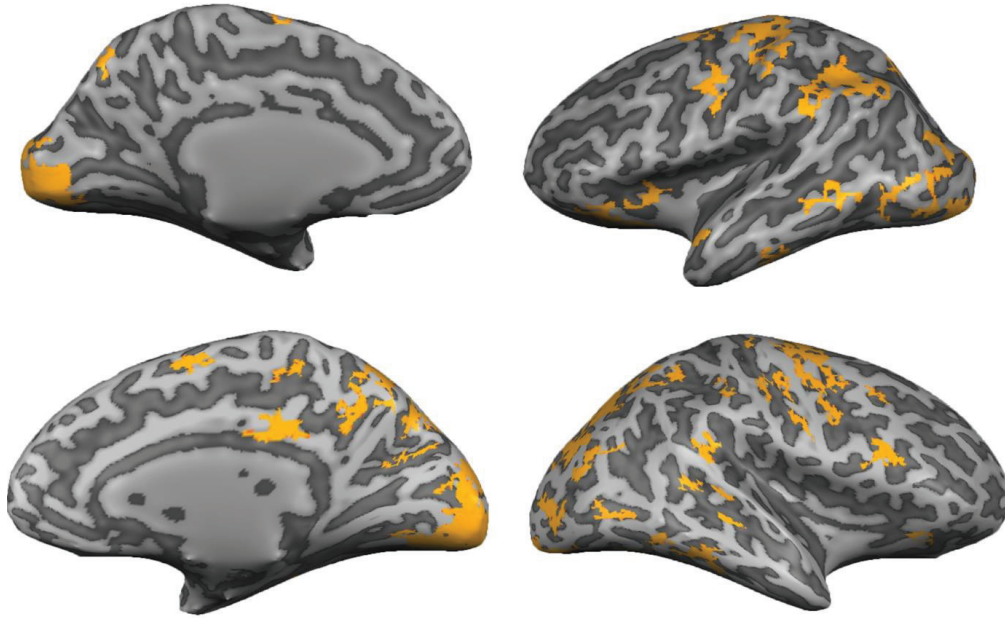
1096  
 1097  
 1098  
 1099  
 1100  
 1101  
 1102  
 1103  
 1104  
 1105  
 1106

**Figure 8. Categorical Biases predict Choice Behavior.** Each plot shows a logistic regression of each orientation channel’s response onto trial-by-trial variability in category judgments. A positive coefficient indicates a positive relationship between an orientation channel’s response and the correct category judgment (i.e., Category B), while a negative coefficient indicates a negative relationship between an orientation channel’s response and correct category judgment (i.e., Category A). Red and blue horizontal lines at the top of each plot depict orientation channels whose estimated  $\beta$  coefficients are significantly below or above zero, respectively (FDR-corrected permutation test;  $p < 0.05$ ). Shaded regions are  $\pm 1$  within-participant S.E.M.





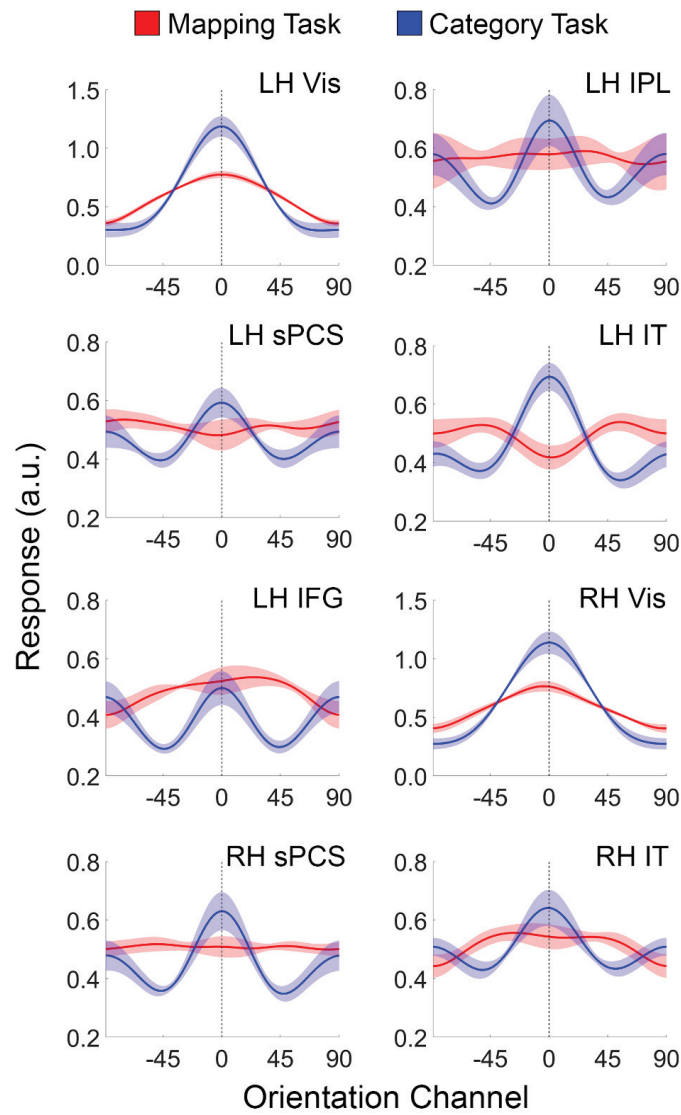
1107 **Figure 9. Category Biases Scale Inversely with Distance from the Category Boundary.** (A)  
 1108 The reconstructions shown in Fig. 3 sorted by the absolute angular distance between each  
 1109 exemplar and the category boundary. In our case, the 15 orientations were bisected into two  
 1110 groups of 7, with the remaining orientation serving as the category boundary. Thus, the  
 1111 maximum absolute angular distance between each orientation category and the category  
 1112 boundary was 48°. Participant-level reconstructions were pooled and averaged across visual  
 1113 areas V1, V2, and V3 as no differences were observed across these regions. Shaded regions are  
 1114  $\pm 1$  within-participant S.E.M. (B) shows the amount of bias for exemplars located 1, 2, 3, or 4  
 1115 steps from the category boundary (quantified via a curve-fitting analysis). Error bars are 95%  
 1116 confidence intervals. a.u., arbitrary units.  
 1117



1118

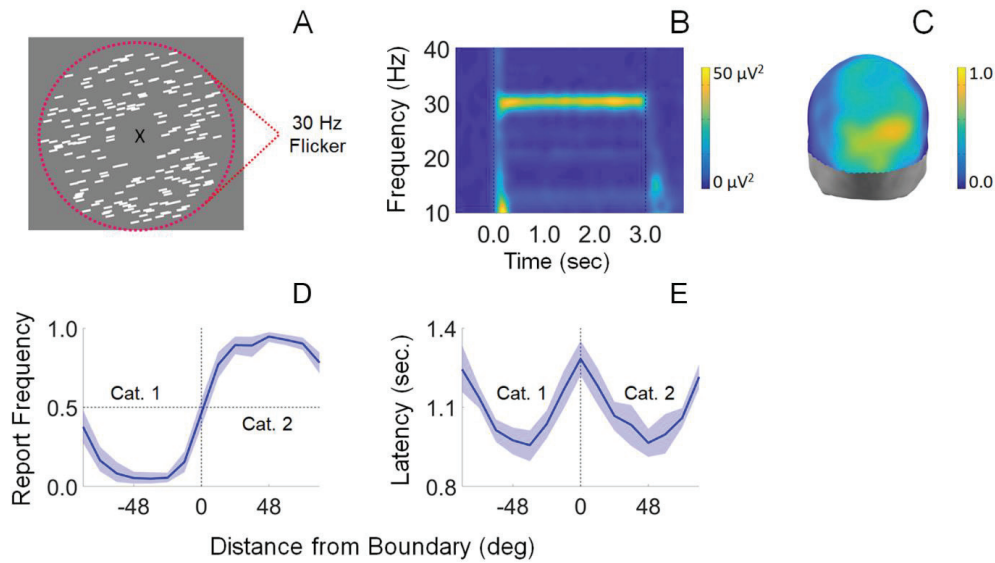
1119

1120 **Figure 10. Cortical Areas Supporting Robust Decoding of Category Information.** We  
1121 trained a linear support vector machine to discriminate between activation patterns associated  
1122 with Category A and Category B exemplars (see *Searchlight Classification Analysis*; Methods).  
1123 The trained classifier revealed robust category information in multiple visual, parietal, temporal,  
1124 and prefrontal cortical areas, including many regions previously associated with categorization  
1125 (e.g., posterior parietal cortex and lateral prefrontal cortex).  
1126



1127  
 1128  
 1129  
 1130  
 1131  
 1132  
 1133  
 1134  
 1135

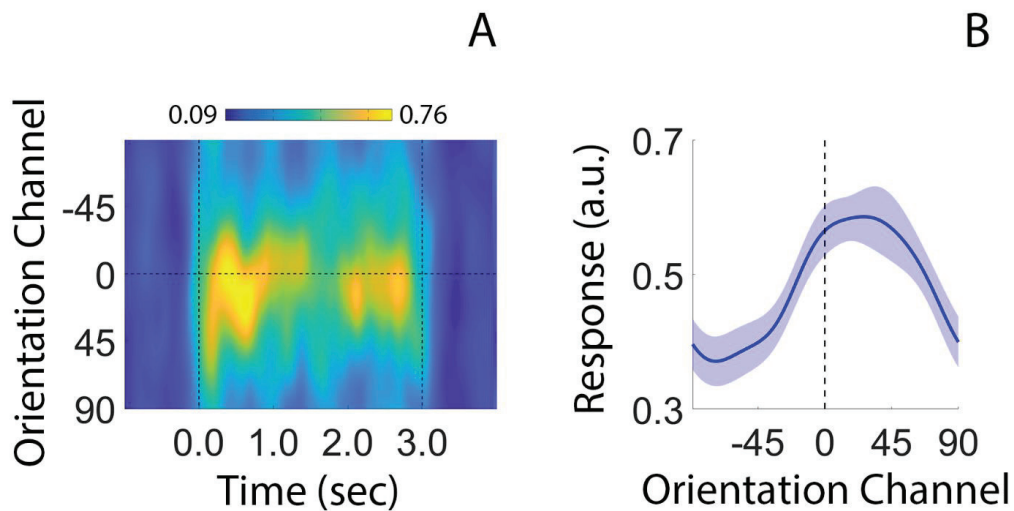
**Figure 11. Stimulus Reconstructions in Visual, Parietal, and Frontal cortical areas during the Orientation Mapping and Categorization Tasks.** During the orientation mapping task, participants detected and reported the identity of a target presented in a stream of letters at fixation. During the categorization experiment, participants categorized stimulus orientation into two discrete groups. Shaded regions are  $\pm 1$  within-participant S.E.M. IPL, inferior parietal lobule; IPS, intraparietal sulcus; sPCS, superior precentral sulcus; IT, inferotemporal cortex, IFG, inferior frontal gyrus. a.u., arbitrary units.



1136  
1137  
1138  
1139  
1140  
1141  
1142  
1143  
1144  
1145  
1146  
1147  
1148

**Figure 12. Summary of Experiment 2.** (A) Participants viewed displays containing an aperture of iso-oriented bars flickering at 30 Hz. (B) The 30 Hz flicker entrained a frequency-specific response known as a steady-state visually-evoked potential (SSVEP). (C) Evoked 30 Hz power was largest over occipitoparietal electrode sites. We computed stimulus reconstructions (Fig. 7) using the 32 scalp electrodes with the highest power. The scale bar indicates the proportion of participants (out of 27) for which each electrode site was ranked in the top 32 of all 128 scalp electrodes. (D-E) Participants categorized stimuli with a high degree of accuracy; incorrect and slow responses were observed only for exemplars adjacent to a category boundary. Shaded regions are  $\pm 1$  within-participant S.E.M.

1149

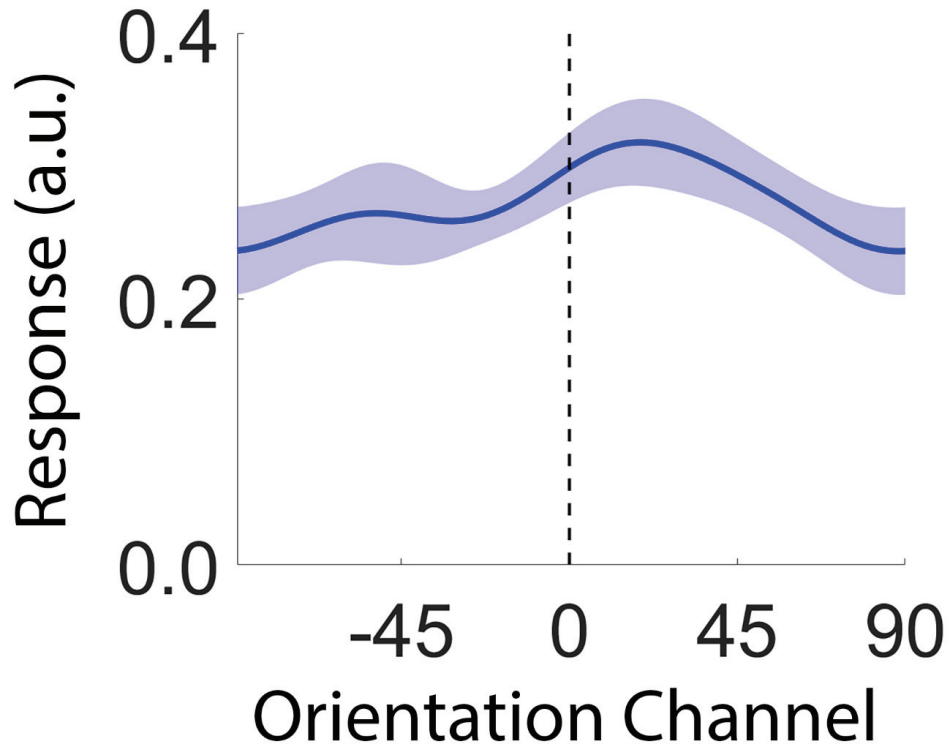


1150

1151 **Figure 13. Category Biases Emerge Shortly after Stimulus Onset.** (A) Time-resolved  
1152 reconstruction of stimulus orientation. Dashed vertical lines at time 0.0 and 3.0 seconds mark  
1153 stimulus on- and offset, respectively. (B) Average channel response function during the first 250  
1154 ms of each trial. The reconstructed representation exhibits a robust category bias ( $p < 0.01$ ;  
1155 bootstrap test). a.u., arbitrary units.

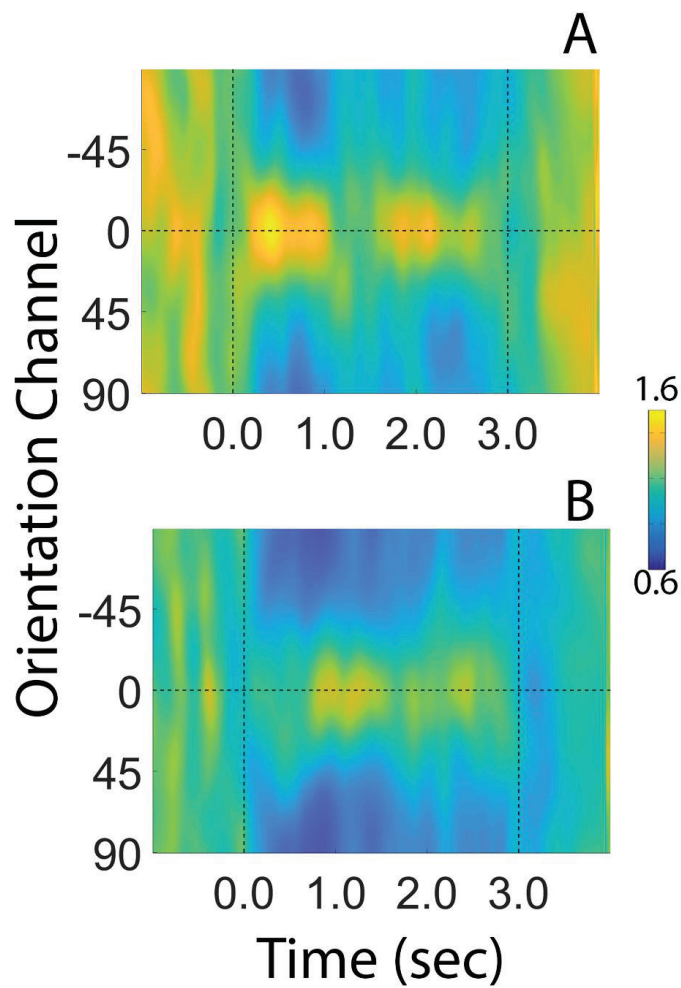
1156

1157



1158  
 1159  
 1160  
 1161  
 1162  
 1163  
 1164  
 1165  
 1166  
 1167  
 1168

**Figure 14. Stimulus- and category information are absent in pre-trial EEG activity.** Time-averaged reconstruction computed over an interval spanning -250 to 0 ms relative to stimulus onset. The center of the reconstruction was statistically indistinguishable from 0° ( $p = 0.234$ ; bootstrap test)



1169  
 1170  
 1171  
 1172  
 1173  
 1174  
 1175  
 1176  
 1177  
 1178  
 1179

**Figure 15. Reconstructions of stimulus orientation during the orientation mapping task (A) and the category discrimination task (B) during Experiment 2.** Vertical dashed lines at time 0.0 and 3.0 mark the start and end of each trial, respectively. Reconstructions were computed using a leave-one-run-out cross validation approach where data from N-1 runs were used to estimate channel weights and data from the remaining run were used to estimate channel responses. This procedure was iterated until all runs had been used to estimate channel responses and the results were averaged over permutations. Units of response are arbitrary.

1180  
1181  
1182  
1183  
1184  
1185  
1186  
1187  
1188  
1189  
1190  
1191  
1192  
1193  
1194  
1195  
1196  
1197  
1198  
1199  
1200  
1201  
1202  
1203  
1204

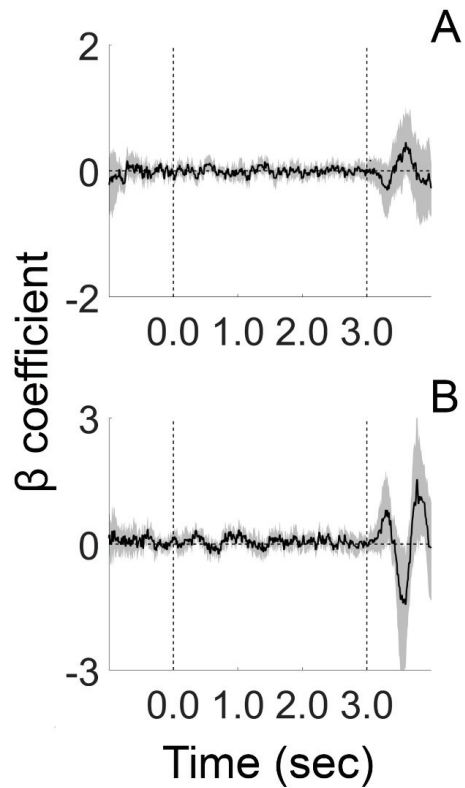
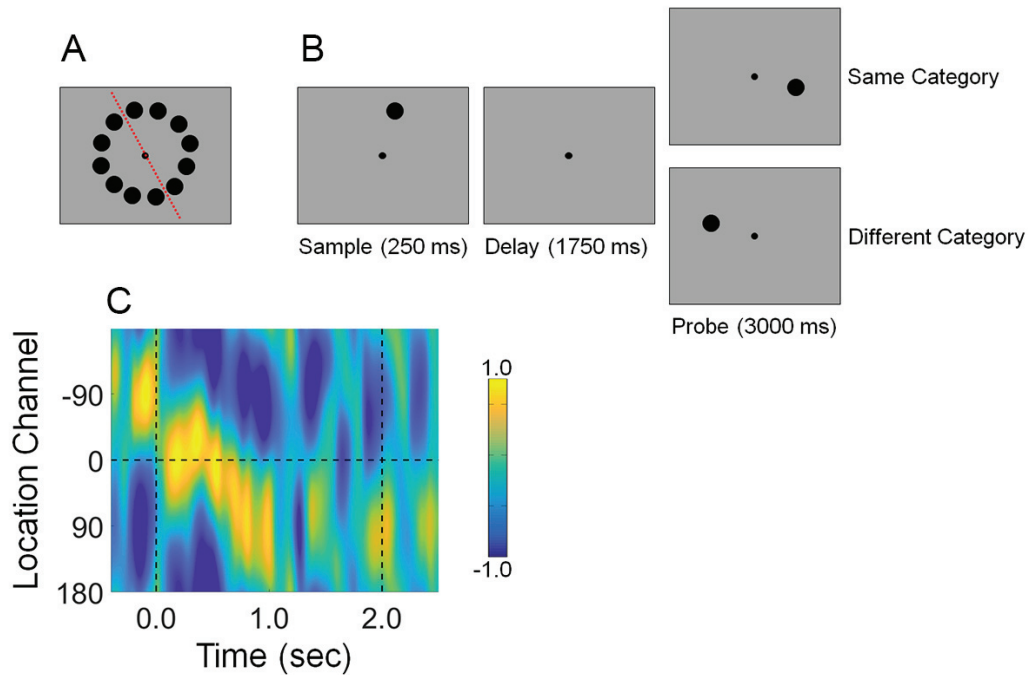


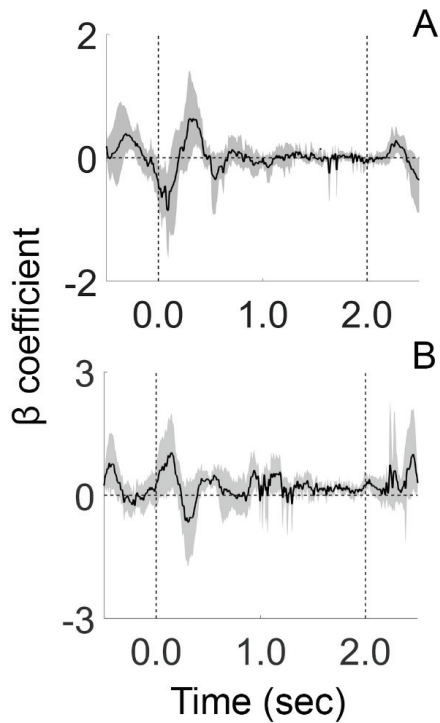
**Figure 16. No systematic biases in eye position during orientation categorization (Experiment 2).** We regressed trial-by-trial records of stimulus orientation (A) or category (B) onto horizontal EOG activity. Thus, positive coefficients reflect a systematic relationship between stimulus orientation (or category) and eye position. No such biases were observed. Black vertical dashed lines at 0.0 and 3.0 depict the start and end of each trial. Shaded regions depict the 95% within-participant confidence interval of the mean.





1205  
1206  
1207  
1208  
1209  
1210  
1211  
1212  
1213  
1214  
1215  
1216  
1217  
1218  
1219

**Figure 17. Design and Results of Experiment 3.** (A) Possible stimulus locations. The orientation of the category boundary (red dashed line) was randomly determined for each participant (example shown). (B) Delayed match-to-category (DMC) task. Participants remembered the position of a sample disc over a blank delay, then judged whether the location of a probe disc was drawn from the same location category or a different location category. In this example, the categories are defined by the boundary shown in panel A. (C) Location-specific reconstructions computed during the DMC task. Vertical dashed lines at 0.0 and 2.0 sec mark the onset of the sample and probe epochs, respectively. Participants could not prepare a response until the onset of the probe display, yet a robust category bias was observed during the delay period. This suggests that category biases observed in Experiments 1 and 2 are not solely due to mechanisms of response selection.



1220

1221 **Figure 18. No systematic biases in eye position during location categorization (Experiment**  
1222 **3).** We regressed trial-by-trial records of stimulus location (A) or category (B) onto horizontal  
1223 EOG activity. Thus, positive coefficients reflect a systematic relationship between stimulus  
1224 orientation (or category) and eye position. No such biases were observed. Black vertical dashed  
1225 lines at 0.0 and 3.0 depict the start and end of each trial. Shaded regions depict the 95% within-  
1226 participant confidence interval of the mean.

1227